Title
The Dissociation Energy and Photochemistry of NO{sub 3}

Journal
Journal of Physical Chemistry, 97(10)

Authors
Davis, H.F.
Kim, B.
Johnston, H.S.
et al.

Publication Date
1992-10-01

LBL-33113
UC-401
Preprint

Lawrence Berkeley Laboratory
UNIVERSITY OF CALIFORNIA

CHEMICAL SCIENCES DIVISION

Submitted to Journal of Physical Chemistry

The Dissociation Energy and Photochemistry of NO_3

H.F. Davis, B. Kim, H.S. Johnston, and Y.T. Lee

September 1992

Prepared for the U.S. Department of Energy under Contract Number DE-AC03-76SF00098

DISCLAIMER

LBL-33113
UC-401

THE DISSOCIATION ENERGY AND PHOTOCHEMISTRY OF NO_3

H. Floyd Davis[a], Bongsoo Kim[b], Harold S. Johnston, and Yuan T. Lee

Department of Chemistry
University of California

and

Chemical Sciences Division
Lawrence Berkeley Laboratory
Berkeley, CA 94720 USA

September 1992

[a]Current Address: Department of Chemistry, University of Southern California, Los Angeles, California 90089-0482.

[b]Current Address: Institute for Molecular Science, Myodaiji, Okazaki 444, Japan.

This work was supported by the Director, Office of Energy Research, Office of Basic Energy Sciences, Chemical Sciences Division, of the U.S. Department of Energy under Contract No. DE-AC03-76SF00098.

ABSTRACT

The photodissociation of NO_3 was studied using the method of molecular beam photofragmentation translational spectroscopy. The existence of two photodissociation channels was confirmed under collision free conditions. At excitation energies below $D_o(O\text{-}NO_2)$ for internally cold NO_3, we observe a large quantum yield (0.70 ± 0.10 at 588 nm) for a concerted 3-center rearrangement resulting in $NO(^2\Pi) + O_2(^3\Sigma_g^-, ^1\Delta)$. The quantum yield for the NO + O_2 channel decreased sharply at wavelengths shorter than 587 nm, falling to <0.01 at 583 nm; while the $NO_2 + O(^3P)$ quantum yield increased to >0.99. Based on this wavelength dependence and the product translational energy distributions, we conclude that the wavelength threshold for NO_3 $(0,0,0,0) \rightarrow NO_2(0,0,0) + O(^3P)$ is 587 ± 3 nm, ie. $D_o(O\text{-}NO_2) = 48.69 \pm 0.25$ kcal/mole. From the enthalpies of formation of $O(^3P)$ and $NO_2(^2A_1)$,[1,2] we calculate $\Delta H_f°(NO_3) = 18.87 \pm 0.33$ kcal/mole at 0 K, and $\Delta H_f°(NO_3) = 17.62 \pm 0.33$ kcal/mole (298 K). This is 2.23 kcal/mole higher than the most recent thermochemical value[3] but is consistent with a value calculated indirectly[4] using the most recent values for the electron affinity[4] (EA) of NO_3 and $\Delta H_f°(NO_3^-)$[5]. Based on the wavelength dependence and translational energy distributions for $NO_3 \rightarrow NO + O_2$, the potential energy barrier for $NO_3(^2A') \rightarrow NO(^2\Pi) + O_2(^3\Sigma_g^-)$ was found to be 47.3 ± 0.8 kcal/mole.

1. INTRODUCTION

An accurate determination of the enthalpy of formation of the nitrate free radical (NO_3) is of considerable importance in properly modelling atmospheric reactions involving nitrogen oxides and ozone. Nearly all thermochemical values of $\Delta_fH°(NO_3)$[1,3,6-9] reported to date rely on the combined results of several separate measurements involving dinitrogen pentoxide (N_2O_5). The most recent thermodynamic measurement of the enthalpy of formation of NO_3 was reported by McDaniel *et. al.*,[3] and led to a value of $\Delta_fH°(NO_3) = 15.39 \pm 0.72$ kcal/mol (298 K). This was within the limits given in the JANAF thermochemical tables[1], but was much lower than the average previously accepted value of 17.0 ± 5.0 kcal/mol[1], suggesting that NO_3 is more stable than was earlier believed. However, Weaver *et al.*[4] directly measured the electron affinity of NO_3, and combined it with a previously determined value for $\Delta_fH°(NO_3^-)$[5], to calculate $\Delta_fH°(NO_3) = 17.9 \pm 0.8$ kcal/mol (298 K). This is inconsistent with the revised thermodynamic value,[3] but falls close to the earlier JANAF recommendation.[1] Other determinations of $\Delta_fH°(NO_3)$ (298 K) ranged from 17.0 to 17.6 kcal/mole (Table I).[6-9] However, those values all relied on the accuracy of a 1957 value[1,10] for $\Delta_fH°(N_2O_5,g)$ (298 K), which, according to McDaniel, *et al.*,[3] is 1.87 kcal/mole too high.

Using the most recent thermodynamic value[3] for $\Delta_fH°(NO_3)$, and the well established[1,2] values for $\Delta_fH°(NO_2)$ and $\Delta_fH°(O^3P)$, we calculate $D_o(O\text{-}NO_2) = 50.92 \pm 0.82$ kcal/mole. This corresponds to a wavelength threshold (0 K) of ~561 nm for $NO_3 \rightarrow NO_2 + O(^3P)$. However, in the earlier room temperature flow cell studies of NO_3 photochemistry published by Magnotta and Johnston[11], the photodissociation channel $NO_3 \rightarrow NO_2 + O(^3P)$ was observed at wavelengths up to 630 nm ($E_{h\upsilon}$ = 45.4 kcal/mole). Since the initial rovibrational energy present in a room temperature sample of NO_3 molecules will, in general, be available for photodissociation, some $NO_2 + O(^3P)$ products are expected to be observed upon excitation at wavelengths somewhat longer than the calculated 0 K threshold of 561 nm. However, Magnotta[11] obtained an O-atom quantum yield of nearly unity at λ = 584 nm. Since it is unlikely that the temperature of the NO_3 radicals generated in their flow cell experiment greatly exceeded room temperature, there should be some vibrational ground state NO_3 present. Based on the calculated value for D_o(O-

NO_2), at 584 nm these molecules should be energetically unable to dissociate to $NO_2 + O(^3P)$. Thus, the recent thermochemical measurements seem to be inconsistent with the $NO_2 + O(^3P)$ quantum yield approaching unity at 584 nm. One possible explanation for the discrepency is that collisional dissociation of excited NO_3 contributed to the observed $O(^3P)$ signal in the photochemical studies at longer wavelengths.[12] Alternatively, there may be a problem with the most recent thermodynamic measurements.

The nitrate radical possesses a structured visible absorption spectrum which has been recorded by a number of groups,[8,13-17] with reasonable agreement in the peak positions and room temperature absorption cross sections. In figure 1, we have reproduced the NO_3 absorption spectrum published by Sander[17] at two temperatures. In 1982, NO_3 fluorescence emission was observed independently by Nelson and coworkers[18], and by Ishiwata *et. al.*,[19] upon laser excitation of NO_3 near the 662 nm $A(^2E') \leftarrow X(^2A')$ band origin. Upon tuning the laser to shorter wavelengths, both groups found that the NO_3 fluorescence excitation spectrum closely matched the known NO_3 absorption spectrum. Since no photochemistry was observed at 662 nm,[8,11] the collision free fluorescence quantum yield is presumably unity. However, the fluorescence intensity dropped to near zero at wavelengths shorter than 605 nm,[18,19] implying the onset of efficient photochemistry. If the calculated 561 nm wavelength threshold for $NO_3 \rightarrow NO_2 + O(^3P)$ is correct, the absence of fluorescence at $\lambda < 605$ nm strongly suggests that the lower energy photodissociation channel forming $NO + O_2$ has a quantum yield near unity at 561 nm $\leq \lambda \leq 605$ nm. This conclusion again conflicts with the earlier photochemical studies[11] which found that the NO quantum yield reached a maximum of ~ 0.4 at 588 nm, dropping sharply to zero to the blue at 584 nm, and falling slowly to zero to the red near 630 nm. If the $NO + O_2$ quantum yield was large over a broader wavelength range than seen by Magnotta, it could be of potential atmospheric significance, since it leads to catalytic destruction of O_3 by *visible* light:[8]

$$NO + O_3 \rightarrow NO_2 + O_2$$
$$NO_2 + O_3 \rightarrow NO_3 + O_2 \qquad (1)$$
$$NO_3 + h\upsilon \rightarrow NO + O_2$$

Net: $2O_3 \rightarrow 3O_2$

The $NO_2 + O$ channel, on the other hand, leads to a null cycle in the balance of atmospheric O_3:

$$NO_2 + O_3 \rightarrow NO_3 + O_2$$
$$NO_3 + h\upsilon \rightarrow NO_2 + O \qquad (2)$$
$$O + O_2 + M \rightarrow O_3 + M$$

Net: Null Cycle

In the NO_3 ($^2E' \leftarrow {}^2A'$) absorption spectrum, Ramsay[14], and Marinelli *et. al.*[20], were unable to resolve rotational structure, even at relatively high resolution. Based on the diffuse absorption spectrum and microsecond NO_3 fluorescence lifetimes, Nelson and coworkers[12] discussed the photochemical dynamics of NO_3 in terms of strong vibronic coupling (Douglas coupling[21]) between the prepared $^2E'$ state and high lying levels of the ground $^2A'$ state. Further evidence for strong vibronic coupling between these electronic states has been obtained by Weaver and coworkers,[4] and Hirota *et. al.*[22] In figure 2, we show the energetics of NO_3 photodissociation, using the JANAF value of $\Delta H_f°(NO_3) = 17.0$ kcal/mole (298 K).[1] Although the process $NO_3 \rightarrow NO + O_2(^3\Sigma^-_g)$ is nearly thermoneutral, a substantial barrier is expected on the potential energy surface.[12,23-25] Siegbahn[23] calculated a barrier as high as 145 kcal/mole for dissociation paths which maintain C_{2v} symmetry. More recently, Boehm and Lohr[25] found that although the barrier height is very sensitive to departure from C_{2v} symmetry, it probably does not lie below 51 kcal/mole. Based on the earlier photochemical studies,[8,11] since the 662 nm band was found to be photochemically inactive, the barrier for formation of $NO + O_2$ must lie above 43.1 kcal/mole. At higher excitation energies, Graham and Johnston,[8] and Magnotta and

Johnston[11] clearly observed NO from NO_3 photolysis. However, there was no determination of the electronic state of the companion O_2 molecule.

We have developed an intense molecular beam source of NO_3 radicals and have investigated the photodissociation of NO_3 using the crossed laser- molecular beam method. By conducting our experiments under the "isolated" conditions of a molecular beam, the possibility of collisional effects are eliminated. Using a "universal" mass spectrometer for product detection,[26,27] competing product channels can be clearly identified and the branching ratios determined. The main focus of this paper is on $D_o(O\text{-}NO_2)$ and the wavelength dependence for the two channels. A more detailed discussion of the photochemical dynamics of NO_3 will appear elsewhere.[28] Our results, which generally agree with the earlier photochemical study of Magnotta,[11] clearly indicate that NO_3 is substantially less stable than implied by the most recent thermochemical measurements[3].

2. EXPERIMENTAL

A continuous NO_3 radical beam was formed by pyrolysis of a 5% N_2O_5/He mixture just prior to supersonic expansion. Dinitrogen Pentoxide (N_2O_5) was synthesized by reaction of NO_2 with excess O_3.[9] The chief design requirements for the pyrolytic NO_3 nozzle source were: 1) to keep the pyrolysis time short to minimize decomposition of NO_3, and 2) to minimize the contribution from vibrationally hot NO_3 by water cooling the nozzle aperture. These considerations led to a the nozzle design shown in Fig 3. The thin walled (0.010") section of the nozzle was resistively heated to ~300°C by passing current (0.6 V, ~100 A) between the front and rear water cooled copper electrodes. Since the thin walled section provided little mechanical strength, the front electrode was supported by a ceramic insulating sleeve. A total gas pressure of ~150 Torr was expanded through the 0.5 mm diameter aperture, resulting in a residence time of <1 msec in the pyrolysis zone. The nozzle temperature and residence time in the pyrolysis region was adjusted to maximize the concentration of NO_3, as monitored by laser induced fluorescence (LIF) intensity near 662 nm,[18,19] or by sampling the beam directly using a mass spectrometer tuned to m/e = 62 (NO_3^+). Comparison of the observed LIF signals

to known NO_3 spectra[17-19] clearly indicated that the fluorescent species in the molecular beam was NO_3. We found that NO_3 shows a parent ion peak (m/e=62), whereas N_2O_5 does not fragment significantly to NO_3^+ upon 200 eV electron bombardment ionization. This provided a second measure of NO_3 concentration which agreed with the LIF measurements. Based on the strong photodissociation signals, we estimate the concentration of NO_3 before expansion to be on the order of 0.1 - 0.5 Torr. Although other species actually dominated the beam, N_2O_5, N_2O_4, NO, and O_2 are transparent[29,30] and NO_2 cannot dissociate by absorption of a single photon[1,2] at the wavelengths studied.

The molecular beam was crossed at 90° by the unfocussed output (2-3 mm dia.) from an excimer pumped dye laser (Lambda-Physik FL2002) operating at wavelengths between 532 and 662 nm (0.2-10 mJ/pulse, 20 ns). The calibration of the laser was checked using a 0.5 m monochromator which was calibrated using a Ne atomic resonance lamp. A small fraction of the photodissociation products travel 37.8 cm to a fixed detector consisting of an electron bombardment ionizer, quadrupole mass filter and Daly ion detector.[26,27] It is important to note that the presence of NO_2 and NO impurities will not result in signal since they are constrained to the beam and will not be detected off axis by the mass spectrometer. The molecular beam could be rotated in a plane perpendicular to the laser axis in order to obtain product time of flight (TOF) spectra at various angles between the molecular beam and detector.[27] A double Fresnel rhomb was used to rotate the laser polarization to measure the product spatial anisotropy. A multichannel scaler, triggered by the laser pulse, was used to record the time of flight spectra. Product translational energy distributions were determined using the forward convolution method using the program CMLAB2, as previously described. [27,31]

3. RESULTS AND DISCUSSION

3.1 Identification of the Primary Processes

The photodissociation of NO_3 was studied at laser wavelengths in the range 532 - 662 nm. At wavelengths near 590 nm, comparable signal levels were observed from both the NO_2

+ O and NO + O_2 channels. Time of flight data was recorded with the mass spectrometer set at O^+(m/e=16), NO^+(m/e=30), O_2^+(m/e=32) and NO_2^+(m/e=46). Near the wavelength threshold for formation of NO_2 + $O(^3P)$, the calculated radius of the Newton circle for the NO_2 fragment will be strongly dependent on the laser excitation wavelength, the true value for D_o(O-NO_2), and the initial internal energy of the NO_3 in the beam. A representative Newton diagram is depicted in figure 4, showing the calculated maximum velocities of the NO-containing fragments resulting from dissociation of internally cold NO_3 at an excitation energy 2 kcal/mole above D_o(O-NO_2). As can be seen from the Newton diagram, the NO_2 from visible photodissociation of NO_3 must be constrained to small detector angles. This constraint results from the proximity of the excitation energy to D_o(O-NO_2), and the heavy NO_2 fragment recoiling from the light O atom. The three larger circles denote the maximum NO velocities corresponding to the three thermodynamically accessible electronic states of O_2. Due to the large amount of available energy, and a large exit potential energy barrier (Fig. 2), a substantial translational energy release is anticipated in the 3-center NO + O_2 channel.

The existence of both the NO_2 + O and NO + O_2 channels at 590 nm is demonstrated in the data shown in Fig 5. The observed NO_2^+ signal results from NO_2 + $O(^3P)$. A similar slow peak was also seen in the NO^+ TOF due to the daughter ion from fragmentation of NO_2 to NO^+ upon electron impact ionization. The fast peak in the NO^+ TOF must be due to NO^+ parent ion from the NO + O_2 channel, since we also observed the momentum-matched O_2 peak at m/e=32 (O_2^+). This is the first direct observation of O_2 from NO_3 photodissociation. Since the signal to noise ratio was better at NO^+ than at NO_2^+, most of the NO_2 + O data was recorded as the NO^+ daughter ion and both product channels could be monitored simultaneously. At 590 nm, the relative intensities of the two NO^+ peaks remained constant as the pulsed laser power was varied from 0.2 - 5 mJ/pulse, and the signal varied linearly with the laser pulse intensity. Since we also obtained similar TOF spectra using a Coherent 699 continuous wave ring dye laser having 10^6 times lower peak power,[28,32] the signal cannot result from multiphoton effects. Additional tests confirmed that the signal results from NO_3: we observed no signal when the nozzle heater was turned off (since N_2O_5 does not absorb in the visible[29]), and no signal was seen when the N_2O_5 was replaced with NO_2.

3.2 Translational Energy Distributions and Branching Ratio at 588 nm.

Figures 6 and 7 show time of flight data recorded with the mass spectrometer tuned to m/e= 30 (NO^+) and m/e = 16 (O^+). The laser wavelength was 588 nm. As expected from the Newton diagram, the NO^+ daughter ion from the NO_2 + O channel is only seen at small detector angles, whereas NO^+ from the NO + O_2 channel is seen at all detector angles. The optimized fits of the translational energy distributions for each channel are shown in figures 8 and 9. The translational energy distribution (P(E)) for the NO + O_2 channel is interesting in that it shows considerable structure due to vibrational excitation of the O_2 product.[28,32] The P(E) for the NO_2 + O channel was found to peak at zero translational energy, but a high energy tail was seen up to ~2.7 kcal/mole. The polarization angle of the laser was rotated with respect to the detector axis using a double fresnel rhomb at a number of photolysis wavelengths. Since we observed no change in the product intensity or shape of the TOF spectra, the product angular distribution is isotropic, ie. the value of the anisotropy parameter[33], β, is zero.

The branching ratio for the NO + O_2 to the NO_2 + O channel at 588 nm may be derived from the fits to the experimental data obtained at m/e = 30 (NO^+) TOF data. The optimized fit of the entire data set acquired at all detector angles yields an "apparent" branching ratio R_{app} defined[34] by equation 3:

$$R_{app} = \frac{\chi(NO+O_2)}{\chi(NO_2+O)} = 2.9 \qquad (3)$$

where the χ's are the integrated areas under the product P(E) distributions for the two different chemical product channels, normalized for the differing Jacobian factors calculated by the computer program in carrying out the CM → LAB coordinate transformations. The actual branching ratio R is related to the "apparent" ratio by the following expression:

$$R = \frac{\phi(NO+O_2)}{\phi(NO_2+O)} = R_{app} \times \frac{\sigma_{ion}(NO_2)}{\sigma_{ion}(NO)} \times \frac{F(NO^+/NO_2)}{F(NO^+/NO)} \qquad (4)$$

In equation 4, $\phi(NO + O_2)$ and $\phi(NO_2 + O)$ are the primary photochemical quantum yields, and $\sigma_{ion}(NO_2)$ and $\sigma_{ion}(NO)$ are the ionization cross sections for NO_2 and NO, respectively. The ionization cross sections were calculated using the following empirical relationship[34,35] relating the peak ionization cross section , $\sigma_{ion}(Å^2)$, to molecular polarizability , α ($Å^3$):

$$\sigma_{ion} = 36\sqrt{\alpha} - 18 \qquad (5)$$

Using the molecular polarizabilities taken from Ref. 36, we calculate σ_{NO2} = 44.5 $Å^2$ and σ_{NO} = 28.9$Å^2$. $F(NO^+/NO_2)$ is the fraction of NO_2 product molecules that fragment to NO^+. The NO_2 fragmentation pattern NO_2^+: NO^+: O^+ in the ionizer was measured in a separate experiment by sampling a 5% NO_2/He beam directly with the mass spectrometer. We found that $F(NO^+/NO_2)$ = 0.51. The published value[37] for $F(NO^+/NO)$ = 0.99 was used in the calculations. By inserting the appropriate values into equation 4, we find that R = 2.3. Since $\phi(NO+O_2) + \phi(NO_2+ O) = 1.0$, we conclude that at 588 nm, under the conditions of our experiment, $\phi(NO+O_2) = 0.7$ and $\phi(NO_2+O) = 0.3$. The primary source of error stems from uncertainty in the P(E) for the NO_2 + O channel for $E_{trans} < 0.2$ kcal/mol, due to our inability to detect very slow photodissociation products within the beam. Some additional uncertainty arises from the values for the ionization cross sections. We estimate that the absolute maximum uncertainty in our NO quantum yield is $\pm$ 0.10. Thus we conclude that for photodissociation of NO_3 at 588 nm, under the conditions of our experiment, $\phi(NO+O_2) = 0.70 \pm 0.10$.

3.3 The NO + O_2 Wavelength Dependence

At wavelengths around 588 nm, the dissociation products are dominated by NO + O_2.

However, upon tuning to shorter wavelengths, the NO + O_2 channel is replaced by NO_2 + O. This is shown in Fig. 10. The shape and position of the NO + O_2 peak near 120 μs (ie. the translational energy distribution) changes very little over this wavelength range.[28,32] Consequently, the sharp decrease in signal intensity for the 120 μs peak upon tuning to 584 nm must result from a sharp decrease in the total flux of NO + O_2 products. We were unable to see *any* NO + O_2 signal at wavelengths in the range 532-583 nm. Based on the high signal to noise ratio in this experiment, our inability to observe NO + O_2 in this range indicates that $\phi(NO + O_2) \leq 0.01$ The integrated area under the TOF spectra for the two peaks, measured at an angle of 10° is shown in Fig. 11. The NO_3 absorption spectrum recorded by Sander[17] is also shown in this wavelength range. Since the NO + O_2 intensity decreased to zero below 583 nm, and because it is known that fluorescence is negligible,[18,19] we conclude that the collision free quantum yield for NO_2 + O reaches $\geq$ 0.99 at 583 nm.

3.4 The wavelength threshold for $NO_3 \rightarrow NO_2 + O(^3P)$

The very large decrease in the NO + O_2 yield, from 0.70 $\pm$ 0.10 at 588 nm to <0.01 at 583nm occurs over a range of photon energies of only 145 cm^{-1} (~0.41 kcal/mole). In this range, the NO_2 + O quantum yield rises from 0.30 $\pm$ 0.10 to $\geq$ 0.99. Such a large change in branching ratios for two competing photochemical channels over a narrow range of photon energies is particularly striking. The most reasonable explanation for this behavior is that the thermodynamic threshold for $NO_3(0,0,0,0) \rightarrow NO_2(0,0,0) + O(^3P)$ exists in this wavelength range. Apparently, upon tuning to shorter wavelengths through this threshold, the rate for simple O-NO_2 bond fission rapidly exceeds that for the concerted three center NO + O_2 channel, and the NO_2 + O quantum yield approaches unity. As suggested by Nelson, *et al.*[12], excitation to the $^2E'$ state at energies above D_o (O-NO_2) probably results in direct dissociation to NO_2 + $O(^3P)$. Based on symmetry considerations,[12,38] this appears to be a very reasonable explanation, since the excited $^2E'$ state correlates directly to ground state $NO_2(^2A_1)$ + $O(^3P)$ (Fig. 2). The NO + O_2 channel, on the other hand, must involve concerted fission of two N-O bonds with simultaneous formation of O=O. The O-O distance in NO_3 is greater than 2.2 Å,[39-41] whereas

that in free O_2 is only 1.208 Å.[42] Consequently, the NO + O_2 channel requires considerable distortion from the NO_3 equilibrium geometry. At 588 nm, the NO_3 molecule is excited only 5.4 kcal/mole above the $^2E'$ (0-0) origin. Since the geometry of NO_3 near the transition state for formation of NO + O_2 is expected to require much more than 5.4 kcal/mole of vibrational energy, the NO + O_2 mechanism must involve internal conversion to high lying levels of a lower electronic state. Since it is known that strong vibronic coupling exists between the $^2E'$ and ground $^2A'$ state,[4,12,22] it is nearly certain that the NO + O_2 channel results from decay of vibrationally hot ground state $NO_3(^2A')$. At excitation energies below $D_o(O\text{-}NO_2)$ the quantum yield for NO + O_2 is large because the NO_2 + $O(^3P)$ channel is energetically closed. Upon reaching threshold for NO_2 + $O(^3P)$, direct dissociation from the excited $^2E'$ state will become the primary photochemical process.

Alternatively, if the NO_3 states above $D_o(O\text{-}NO_2)$ have strongly mixed $^2A'$ and $^2E'$ character, and both channels result from internal conversion of NO_3, a model involving competing channels in decay of a vibrationally excited molecule might be appropriate. In this case, the branching ratio will be determined by the geometric A-factors for the transition states, the height of the potential energy barrier for NO + O_2, and $D_o(O\text{-}NO_2)$.[43] Based on our observations, if both dissociation processes are from vibrationally hot ground state NO_3, the sharp rise in the NO_2 yield upon tuning the laser over an energy range of only <0.41 kcal/mol would imply that the A-factor for simple O-NO_2 bond rupture must greatly exceed that for the concerted three center rearrangement producing NO + O_2. Since the NO_3 $^2E'$ excited state correlates directly to NO_2 + $O(^3P)$, and because the energy range over which both channels appear to be in competition is extremely narrow, it seems much more reasonable that the NO_2 + $O(^3P)$ channel is a direct process from the excited $^2E'$ state.

The exact location of the threshold for dissociation of cold NO_3 to NO_2 + $O(^3P)$ can be estimated based on figure 11. Comparing the NO + O_2 intensity to the absorption cross section, upon tuning below 589 nm, the NO intensity follows the NO_3 absorption profile, but it drops sharply at 586 nm. Based on this, the wavelength threshold for NO_2 + O appears to lie very close to 587 nm. Several observations allow us to place error limits on this quantity. At 584

nm, the NO + O_2 yield has dropped to <0.05, and so $\phi(NO_2 + O) > 0.95$. As we will see below, more than 5% of the beam is in its vibrational ground state, so $\lambda_{thr} \geq 584$ nm. As shown in Fig. 11, the NO signal intensity reaches a maximum at 589 nm. This is also a local peak in the room temperature NO_3 absorption cross section.[17] However, the exact location of the absorption peak in the bulk and molecular beam might differ slightly due to the effect of rotational cooling. If the peak in the molecular beam absorption cross section was shifted slightly to the blue of 589 nm, say to 587 nm, it is possible that the decreased NO signal that we observed below 589 nm actually results from the threshold lying near 589 nm. Since the NO_3 absorption cross section has not been measured under beam conditions, we cannot rule out this possibility. Based on the increased NO + O_2 signal upon tuning from 590 to 589 nm, however, the threshold wavelength for $NO_2 + O(^3P)$ cannot be above 590 nm. Thus, we conclude that the wavelength threshold for $NO_3(0,0,0,0) \rightarrow NO_2(0,0,0) + O(^3P)$ is 587 ± 3nm, and so $D_o(O\text{-}NO_2) = 48.69 \pm 0.25$ kcal/mole. Of course, we are assuming that there is no potential energy barrier for dissociation of NO_3 to $NO_2 + O(^3P)$ in excess of $D_o(O\text{-}NO_2)$. This is confirmed by our translational energy distributions (P(E)) for the $NO_2 + O(^3P)$ products, as discussed in sections 3.5 and 3.6.

We have obtained a quantum yield for $NO_3 \rightarrow NO_2 + O(^3P)$ of 0.30 ± 0.10 at 588 nm. Since we found that the wavelength threshold for $NO_3(0,0,0,0) \rightarrow NO_2 + O$ is 587 nm, the $NO_2 + O$ products formed at all wavelengths longer than 587 nm must result from photolysis of internally excited NO_3. Under the conditions of our experiment, this internal energy must be primarily vibrational energy because of efficient rotational cooling in the supersonic expansion. Since the quantum yield for NO + O_2 is 0.70 ± 0.10 at 588 nm, we conclude that $\sim$70% of the molecules absorbing at 588 nm are in their ground vibrational state. The remaining $\sim$30% have at least 1 quantum of vibrational excitation. At 588 nm they will be excited to a level above $D_o(O\text{-}NO_2)$ and will dissociate to the dynamically more favorable products, $NO_2 + O(^3P)$.

The shift in branching ratios upon tuning through $D_o(O\text{-}NO_2)$ is particularly abrupt in our experiment. This is partly due to cooling of NO_3 rotational energy upon supersonic expansion.

Near threshold for NO_2 + $O(^3P)$, the actual branching ratios for a bulk sample having a Boltzmann distribution of vibrational and rotational energies will depend very strongly on the temperature. This is because it is the *total energy* of the excited NO_3 molecule, E_{int} + $E_{h\nu}$, relative to $D_o(O\text{-}NO_2)$ that controls the identity of the products. The vibrational frequencies[19,22,40,41] for NO_3, assuming D_{3h} structure are shown in Table II, together with calculated populations at two temperatures. Due to the low vibrational frequencies for NO_3, even at room temperature a significant fraction of the molecules will have some vibrational excitation. Assuming a Boltzmann distribution, the probability of finding a vibrationless NO_3 molecule in a 25°C sample is calculated to be ~0.65, and ~23% of the molecules will have one quantum of υ_4 (363cm^{-1}) excitation. In addition to vibrational energy, rotational excitation in a bulk room temperature sample can contribute several kcal/mole to the internal energy. A substantial fraction of this will, in general, be available for photodissociation. Thus, the effect of initial NO_3 temperature on the branching ratio near 588 nm should be quite dramatic. This is illustrated by comparing our beam results to the earlier flow cell results of Magnotta.[11] We have obtained an NO + O_2 quantum yield of 0.70 ± 0.10 at 588 nm, whereas Magnotta's flow cell value was only ~0.25 at this wavelength. This difference is quite reasonable, assuming that the NO_3 radicals in Magnotta's experiment were near room temperature. It appears that absorption by NO_3 radicals having a thermal distribution of vibrational and rotational energy explains the substantial quantum yield for NO_2 + O in the gas cell experiment at wavelengths considerably to the red of the 0 K 587 nm threshold.

In order to gauge the role that thermally excited molecules will play in determining the quantum yields for a room temperature sample, we consider the temperature dependence of the NO_3 absorption spectrum, published by Sander[17] (Figs 1 & 11). It was found that throughout most of the spectrum, the NO_3 absorption cross sections increased with decreasing temperature. Such behavior is expected when the Franck-Condon factors for absorption from the ground state of NO_3 are greater than from higher vibrational levels. Peaks primarily from hotband absorption were clearly observed at 637 nm and 678 nm. These are 363cm^{-1} to the red of the 623nm and 662nm peaks, and absorption increased with temperature.[17] As shown in Figs. 1, and 11, the NO_3 absorption cross section near 588 nm shows a temperature dependence which is similar to

that seen at most other wavelengths. Based on our molecular beam measurement, at 588 nm, approximately 30% of the absorption cross section results from excitation of internally hot molecules. Based on Magnotta's work, this fraction increases to ~75% in a room temperature gas cell. Since the temperature dependence at this wavelength is typical of the entire spectrum (Figs. 1, 11) the absorption due to internally excited NO_3 appears to be nearly continuous across the entire spectrum. Our measurements of the NO_2 + $O(^3P)$ translational energy distributions across a wide range of wavelengths (Section 3.5) are consistent with this conclusion. In fact, we have been unable to find any wavelength in the range 570-596 nm where hotband activity makes no contribution.

3.5. NO_2 + $O(^3P)$ Translational Energy Distributions At Other Wavelengths.

Time of flight data for the NO_2 + $O(^3P)$ products was obtained with the mass spectrometer set at NO_2^+, NO^+, and O^+ at a number of laser wavelengths. The NO^+ and O^+ TOF data from 570 nm photodissociation of NO_3 is shown in figure 12, and the optimized P(E) is shown in figure 13. Time-of-flight data and the corresponding P(E) for 548 nm photodissociation of NO_3 are shown in figures 14 and 15. At both wavelengths, the P(E) peaks at or near zero translational energy, with the P(E) gradually decreasing at higher energies.

In the photodissociation of an isolated NO_3 molecule, conservation of energy dictates that:

$$E_{photon} + E_{int,NO_3} = D_o(O\text{-}NO_2) + E_{trans,NO_2+O} + E_{int,NO_2} + E_{int,_O} \qquad (6)$$

For a simple bond rupture, such as $NO_3 \rightarrow NO_2$ + $O(^3P)$, the maximum translational energy reease corresponds to the production of internally cold fragments,[27] i.e:

$$E_{photon} + E_{int,max,NO_3} = D_o(O\text{-}NO_2) + E_{trans,max,NO_2+O} \qquad (7)$$

Since the photon energy is known, by measuring the maximum translational energy for the NO_2 + O products, we obtain $D_o(O\text{-}NO_2)$ - $E_{int,max,\,NO3}$ directly:

$$D_o(O\text{-}NO_2) - E_{int,max,NO_3} = E_{photon} - E_{trans,max,NO_2+O} \qquad (8)$$

If the NO_3 was efficiently cooled to 0 K, then $E_{int,max,NO3} \sim 0$ and $D_o(O\text{-}NO_2)$ could be obtained directly from equation 8. However, based on the substantial NO_2 + $O(^3P)$ quantum yield that we observe at photon energies below the 0K threshold (587 $\pm$ 3 nm), it is clear that a fraction of the molecules in the beam do have some vibrational excitation. Photodissociation of these molecules could result in products having larger translational energy release than would be seen from internally cold molecules.

Based on our value for $D_o(O\text{-}NO_2)$ = 48.69 $\pm$ 0.25 kcal/mole obtained in section 3.4, for a given wavelength, one can easily calculate the maximum NO_2 + $O(^3P)$ translational energy from photodissociation of internally cold NO_3. The maximum translational energy is calculated to be 1.45 $\pm$ 0.25 kcal/mole at 570 nm, and 3.45 $\pm$ 0.25 kcal/mole at 548 nm. These limiting values are indicated on the P(E) in Figs. 13 and 15. At both wavelengths, a small fraction of the products appear with energies above this limit. Based on the integrated areas under the P(E) above these limits, at 570 nm approximately 12% of the products have $E_{trans} \geq 1.45$ kcal/mole, and at 584 nm, approximately 5% have $E_{trans} \geq$ 3.45 kcal/mole. These products must result from photodissociation of internally excited NO_3 radicals. Since photodissociation of internally excited NO_3 could also lead to slower, more internally excited NO_2 + O products, these values of 12% and 5% represent lower limits to the hotband contributions at the two wavelengths, under our experimental conditions. This behavior is quite representative of all wavelengths where we have studied NO_3 photodissociation. Although most products are formed with translational energies below the calculated maximum for photodissociation of ground state NO_3, there is a higher energy contribution from internally excited molecules.

3.6 Potential Energy Barriers for $NO_3 \rightarrow NO_2 + O(^3P)$ and $NO_3 \rightarrow NO + O_2(^3\Sigma_g^-)$

As shown in figures 13 and 15, the P(E) for the $NO_2 + O$ channel peaks at zero energy, as expected for simple bond rupture without an exit barrier in excess of $D_o(O\text{-}NO_2)$.[44] The conclusion that there is no exit barrier for the $NO_2 + O(^3P)$ reaction is of considerable importance in determining $D_o(O\text{-}NO_2)$. We have ascribed the sharp decrease in the $NO + O_2$ yield and concomitant increase in the $NO_2 + O$ channel near 587 nm as due to the energy threshold for $NO_2 + O(^3P)$. If, in fact, there was a potential energy barrier above $D_o(O\text{-}NO_2)$ in the exit channel, then our wavelength threshold would correspond to the barrier height and our value for $D_o(O\text{-}NO_2) = 48.69 \pm 0.25$ kcal/mole would be an upper limit. Since the barrier is zero, the reverse reaction $O(^3P) + NO_2 \rightarrow NO_3$ will proceed without an activation energy. This is not at all surprising for a radical recombination process.[45]

The data shown in figure 8 strongly suggests that there is a large yield of $O_2(^1\Delta)$ from photodissociation of NO_3 at 588 nm. However, based on the integrated area of the P(E) with $E_{trans} > 25$ kcal/mole, we conclude that at least 15% of the O_2 is formed in the ground $^3\Sigma_g^-$ state at 588 nm. Since we clearly observe[28,32] a substantial yield of $NO + O_2(^3\Sigma_g^-)$ at 594 nm, an absolute upper limit to the height of the potential energy barrier for $NO_3 \rightarrow NO + O_2(^3\Sigma_g)$ is 48.1 kcal/mole. The $NO + O_2$ signal intensity decreases substantially above 600 nm, and becomes very weak at 605 nm. It appears that the signal at 605 nm may primarily result from hotband absorption. We were unable to observe *any* $NO + O_2$ products under the local peak at 613 nm, or at longer wavelengths. Based on the absence of $NO + O_2$ from photolysis of NO_3 at 613 nm, a lower limit to the barrier height is 46.6 kcal/mole. Since the $NO + O_2$ channel results from internal conversion to high lying vibrational levels of the ground $NO_3(^2A')$ state (Section 3.4), we conclude that the height of the potential energy barrier for $NO_3(^2A') \rightarrow NO + O_2(^3\Sigma_g^-)$ is 47.3 ± 0.8 kcal/mole.

Although the reaction $NO + O_2(^3\Sigma_g^-) \rightarrow NO_2 + O(^3P)$ is endothermic by ~ 47 kcal/mole, NO is rapidly converted to NO_2 in the atmosphere. This reaction must involve an intermediate species, either NO_3 or N_2O_2.[23] Whether or not the intermediate is symmetric NO_3 will depend[23]

on the height of the potential energy barrier for the following reaction:

$$NO + O_2(^3\Sigma_g) \rightarrow NO_3(^2A') \qquad \Delta H = 2.59 \pm 0.37 \text{ kcal/mole} \qquad (9)$$

By subtracting the reaction endothermicity from the above photochemically determined barrier height for NO_3 photodissociation, we conclude that the barrier height for reaction 9 is 44.7 ± 1.2 kcal/mole. Although this is far too high for the reaction to be important at thermal energies, our experimentally determined value is much lower than the previous theoretical estimates, which have been as high as 145 kcal/mole. [23-25]

Our photochemical results provide some insight into the dynamics of reaction 10:

$$O(^3P) + NO_2 \rightarrow [NO_3]^{\ddagger} \rightarrow NO + O_2, \qquad (10)$$

In 1961, Clyne and Thrush[46] found that reaction of ^{18}O with $N^{16}O_2$ led to formation of $N^{18}O$ and $^{18}O^{16}O$, with the probability of finding ^{18}O in the O_2 product two times higher than in NO. Based on this, it was concluded that the reaction intermediate has three equivalent oxygen atoms; ie: it is *sym-* NO_3, rather than OO-NO. For this mechanism to be valid, the potential energy barrier for $NO_3 \rightarrow NO + O_2(^3\Sigma_g)$ must be smaller than $D_o(O\text{-}NO_2)$; otherwise the reaction rate could not be as large as experimentally measured.[47-51] Since it was previously thought that the barrier was probably much higher than $D_o(O\text{-}NO_2)$, the three center mechanism of Clyne and Thrush was disfavored by some.[50,51] However, based on our work, since the barrier height is clearly lower than $D_o(O\text{-}NO_2)$, it appears quite reasonable that the $O(^3P) + NO_2$ reaction could involve a symmetric NO_3 intermediate.

3.7. Calculation of $\Delta_f H°(NO_3)$, (298 K)

Based on the wavelength threshold of 587 ± 3 nm for $NO_3(0,0,0,0) \rightarrow NO_2 + O(^3P)$, we calculate $D_o(O\text{-}NO_2)=48.69 \pm 0.25$ kcal/mole. In order to calculate $\Delta_f H°(NO_3)$, 0 K, we require values for $\Delta_f H°(O^3P)$, and $\Delta_f H°(NO_2)$. According to the JANAF tables[1], $\Delta_f H°(O^3P)$

= 58.98 ± 0.02 kcal/mol (0 K). Based on photochemical studies, the energy threshold for dissociation of ground state NO_2 to NO + $O(^3P)$ is 71.860 ± 0.002 kcal/mol.[2] Using the JANAF values[1] for $\Delta_fH°(NO)$ = 21.46 ± 0.04 kcal/mol (0 K), we calculate $\Delta_fH°(NO_2)$ = 8.58 ± 0.06 kcal/mol (0 K). This is nearly identical to the JANAF value of 8.59 ± 0.19 kcal/mol (0 K), but the error limits are considerably smaller. From our value for $D_o(O\text{-}NO_2)$, we calculate $\Delta_fH°(NO_3)$ = 18.87 ± 0.33 kcal/mole at 0 K. Based on published heat capacity corrections[52] which agree with those we calculate according to Herzberg,[53] our value corresponds to a room temperature value of $\Delta_fH°(NO_3)$ = 17.62 ± 0.33 kcal/mole (298 K). Our result is in good agreement with a value recently calculated by Weaver et al.[4] Using their value[4] for the NO_3 electron affinity (3.937 ± 0.018 eV) measured by photodetachment of NO_3^- , and a previously determined[5] value of $\Delta_fH°(NO_3^-)$, they calculated $\Delta_fH°(NO_3)$ = 17.9 ± 0.8 kcal/mole (298 K).

Based on the thermochemical measurements of McDaniel,[3] the wavelength threshold for $NO_3 \rightarrow NO_2 + O(^3P)$ is predicted to be 561 nm, whereas we have found that the collision free quantum yield for this channel reaches >0.99 at a much longer wavelength, 583 nm. The thermochemical work on NO_3, which has been subsequently employed in two separate publications,[38,52] also led to a revised value of $\Delta_fH°(N_2O_5,g)$ = 1.19 ± 0.6 kcal/mole (298 K).[3] The substantial revision in that quantity was in large part responsible for the large difference between their calculation of $\Delta_fH°(NO_3)$ = 15.39 ± 0.75 kcal/mole (298 K)[3] and the earlier JANAF value of $\Delta_fH°(NO_3)$ = 17.0 ± 5.0 kcal/mole (298 K).[1] Our value for $\Delta_fH°(NO_3)$, as well as that of Weaver *et. al.*,[4] do *not* rely on the accuracy of $\Delta_fH°(N_2O_5,g)$. As shown in Table I, these two determinations are in excellent agreement with a number of earlier values for $\Delta_fH°(NO_3)$.[6-9] These earlier values were based on the JANAF value[1] of $\Delta_fH°(N_2O_5,g)$ = 2.70 ± 0.31 kcal/mole (298 K), which dates back to the 1958 work of Ray and Ogg.[10] The good agreement between our value and the earlier values for $\Delta_fH°(NO_3)$ suggests that the JANAF value[1] for $\Delta_fH°(N_2O_5)$ is probably correct.

An accurate knowledge of $\Delta_fH°(NO_3)$ is important in calculations pertaining to atmospheric reactions. The consequences of small errors in this quantity can have substantial effects, particularly in reactions that are nearly thermoneutral. For example, by using our value,

the equilibrium constant for $NO_3 + HCl \rightleftarrows HNO_3 + Cl$ is calculated to be approximately *50 times larger* than the value based on the earlier thermodynamic data.[3]

4. CONCLUSIONS

We have generated an NO_3 radical beam and have studied the photodissociation of NO_3 at a range of laser wavelengths. Based on the sharp drop in $NO + O_2$ quantum yield near 587nm, and translational energy measurements on the $NO_2 + O(^3P)$ products, we conclude that $D_o(O\text{-}NO_2) = 48.69 \pm 0.25$ kcal/mole and $\Delta_f H°(NO_3) = 17.62 \pm 0.33$ kcal/mole (298 K). Our results show that for a "cold" sample of NO_3, the $NO + O_2$ channel dominates near 588 nm. However, this quantum yield will be diminished significantly by thermal excitation of the parent NO_3 and the branching ratio for the two processes near 588 nm will be strongly temperature dependent. In basic agreement with the earlier work by Magnotta,[11] the simple fission channel $NO_3 \rightarrow NO_2 + O(^3P)$ channel has a primary quantum yield of 1.0 for $532 \leq \lambda \leq 583$ nm. Although they detected $NO_2 + O$ at wavelengths up to ~630 nm, this signal appears to be largely due to contributions from thermally populated rovibrational levels of NO_3 present in the room temperature flow cell. After allowing for the effect of internal energy on the photodissociation quantum yields, our beam results seem to be consistent with the room temperature flow cell results, and it appears that the photochemical parameters derived from Magnotta's work should be correct for a room temperature NO_3 sample.

5. ACKNOWLEDGEMENTS

The NO_3 nozzle used in these experiments was designed in collaboration with Dr. Matt Cote, Jim Myers, and James Chesko. H.F.D. thanks Jim Myers for an improved version of CMLAB2 and acknowledges useful discussions with Dr. Alex Weaver and Prof. Daniel Neumark. We also thank Dr. Randall Boehm for preprints of his theoretical work and a copy of his Ph.D. thesis. H.F.D. thanks NSERC (Canada) for a 1967 Science and Engineering

Fellowship. Some of the equipment used in this work was provided by the Office of Naval Research under Contract No. N00014-89-J-1297. This work was supported by the Director, Office of Energy Research, Office of Basic Energy Sciences, Chemical Sciences Division of the U.S. Department of Energy under Contract No. DE-AC03-76F00098.

6. REFERENCES

1. Chase, M.W. Jr.; Davies, C.A.; Downey, J.R.; Frurip, D.J.; McDonald, R.A.; Syverud, A.N. J. Phys. Chem. Ref. Data. **1985,** 14, Supp. 1. (*JANAF Thermochemical Tables, 3rd. ed.*)
2. Robra, U.; Zacharias, H.; Welge, K.H. Z. Phys. D. **1990**, 16, 175.
3. a) McDaniel, A.H.; Davidson, J.A.; Cantrell, C.A.; Shetter, R.E.; Calvert, J.G. J. Phys. Chem. **1988**, 92, 4172 .
   b) Cantrell, C.A.; Davidson, J.A.; McDaniel, A.H.; Shetter, R.E.; Calvert, J.G.; J. Chem. Phys. **1988**, 88, 4997.
4. Weaver, A.; Arnold, D.W.; Bradforth, S.E.; Neumark, D.M. J. Chem. Phys. **1991**, 94, 1740.
5. Davidson, J.A.; Fehsenfeld, F.C.; Howard, C.J. Int. J. Chem. Kin. **1977**, 9, 17.
6. Burrows, J.P.; Tyndall, G.S.; Moortgat, G.K. Chem. Phys. Lett **1985**, 119, 193.
7. Kircher, C.C.; Margitan, J.J.; Sander, S.P. J. Phys. Chem. **1984**, 88, 4370.
8. a) Graham, R.A.; Johnston, H.S. J. Phys. Chem, **1978**, 82, 3, 254.
   b) Graham, R.A., Ph.D. Thesis, University of California, Berkeley, **1978**. Lawrence Berkeley Laboratory Report LBL- 4147.
9. Schott, G.; Davidson, N. J. Am. Chem. Soc. **1958**, 80, 1841.
10. Ray, J.D.; Ogg, R.A.,Jr., J. Chem. Phys. **1957**, 26, 984.
11. a) Magnotta, F.; Johnston, H.S. Geophys. Res. Lett. **1980**, 7, 769.
    b) Magnotta, F. Ph.D. Thesis, University of California, Berkeley, **1979**. Lawrence Berkeley Laboratory Report LBL-9981.
12. Nelson, H.H.; Pasternack, L.; McDonald, J.R. J. Chem. Phys. **1983**, 79, 4279.

13. Jones, E.J.; Wulf, O.R. J. Chem. Phys., **1937**, 5, 873.
14. Ramsay, D.A. Proc. Colloq. Spect. Int. **1962**,10, 583.
15. Ravishankara, A.R.; Mauldin, R.L. J. Geophys. Res., **1986**, 91, 8709.
16. Ravishankara, A.R.; Wine, P.H. Chem. Phys. Lett. **1983**, 101, 73.
17. Sander, S.P. J. Phys. Chem. **1986**, 90,4135.
18. Nelson, H.H.; Pasternack, L.; McDonald, J.R. J. Phys. Chem. **1983**, 87, 1286.
19. Ishiwata, T.; Fujiwara, I. Naruge, Y.; Obi, K.; Tanaka, I. J. Phys. Chem. **1983**, 87, 1349.
20. Marinelli, D.J.; Swanson, D.M.; Johnston, H.S.; J. Chem. Phys. **1982**, 76, 2864.
21. Douglas, A.E., J. Chem. Phys., **1966**, 45, 1007.
22. Hirota, E., Kawaguchi, K., Ishiwata, T., Tanaka, I., J. Chem. Phys. **1991**, 95(2), 771.
23. Siegbahn, Per E.M. J. Compt. Chem. **1985**, 6,3,182.
24. Pearson, R.G., Pure App. Chem. **1971**, 27, 145.
25. Boehm, R.C., Ph.D. Thesis, University of Michigan, **1990**.
26. Lee, Y.T.; McDonald, J.D.; LeBreton, P.R.; Herschbach, D.R. Rev. Sci. Instrum. **1969**, 40,1402.
27. Wodtke, A.M.; Lee, Y.T. J. Phys. Chem. **1985**, 89, 4744.
28. Davis, H.F.; Kim, B.; Johnston, H.S.; Lee, Y.T. to be published.
29. Johnston, H.S.; Graham, R.A. Can. J. Chem. **1974**,52, 1415.
30. Okabe, H., *Photochemistry of Small Molecules,* J. Wiley and Sons, Inc., **1978**.
31. Minton, T.K.; Nathanson, G.M.; Lee, Y.T. J. Chem. Phys., **1987**, 86(4), 1991.
32. Davis, H.F. Ph.D. Thesis, University of California, Berkeley, **1992**. Lawrence Berkeley Laboratory Report LBL-32515.
33. Zare, R.N. Mol. Photochem. **1972**, 4,1.
34. a) Krajnovich, D.; Butler, L.J.; Lee, Y.T. J. Chem. Phys., **1984**, 81, 3031.
    b) Wodtke, A.M.; Hintsa, E.J.; Lee, Y.T. J. Phys. Chem. **1986**, 90, 3549.
35. Center, R.E.; Mandl, A. J. Chem. Phys., **1972**, 57, 4104.
36. Weast, R.C., Ed., *CRC Handbook of Chemistry and Physics,* CRC Press, Inc.

Boca Raton, Fla. **1987.**

37. Stenhagen, E.; Abrahamsson, S.; McLafferty, F.W.; *Atlas of Mass Spectral Data,* Interscience Pub., N.Y. **1969.**
38. Wayne, R.P.; Barnes, I.; Biggs, P.; Burrows, J.P.; Canosa-Mas, C.E.; Hjorth, J.; Le Bras, G.; Moortgat, G.K.; Perner, D.; Poulet, G.; Restelli, G.; Sidebottom, H.; *The Nitrate Radical: Physics, Chemistry, and the Atmosphere 1990,* Air Pollution Research Report 31, **1990.**
39. Assuming D_{3h} symmetry and an equilibrium N-O bond length of 1.240Å. (Refs. 40,41).
40. Ishiwata, T.; Tanaka, I.; Kawaguchi, K.; Hirota, E.; J. Chem. Phys. **1985**, 82, 2196.
41. Friedl, R.R, Sander, S.P. J. Phys. Chem. **1987**, 91, 2721.
42. Huber, K.P.; Herzberg, G.; *Molecular Spectra and Molecular Structure IV, Constants of Diatomic Molecules,* Van Nostrand Reinhold Co, **1979.**
43. See, eg. Robinson, P.J., Holbrook, K.A., *Unimolecular Reactions* , Wiley, New York, **1972.**
44. Sudbo, Aa. S.; Schulz, P.A., Grant, E.R.; Shen, Y.R.; Lee, Y.T. J. Chem. Phys., **1979,** 70, 912.
45. Johnston, H.S. *Gas Phase Reaction Rate Theory*, Ronald Press, New York, **1966.**
46. Clyne, M.A.A.; Thrush, B.A. Trans. Faraday Soc. **1962**, 58, 511.
47. a) Ongstad, A.P.; Birks, J.W. J. Chem. Phys. **1986**, 85, 3359.
    b) Ongstad, A.P.; Birks, J.W. J. Chem. Phys. **1984**, 81, 3922.
48. Geers-Muller, R.; Stuhl, F. Chem. Phys. Lett. **1987,** 135, 263.
49. Davis, D.D.; Herron, J.T., Huie, R.E., J. Chem. Phys., **1973**, 58, 530.
50. Benson, S.W., J. Chem. Phys., **1963**, 38, 1251.
51. Clyne, M.A.A.; Thrush, B.A. J. Chem. Phys., **1963**, 38, 1252.
52. Abramowitz, S., Chase, M.W. Jr. Pure and Appl. Chem. **1991**, 63(10). 1449.
53. Herzberg, G., *Infrared and Raman Spectra* , Van Nostrand Reinhold Co., N.Y., **1945.**

Table I: Summary of Experimental Values for $\Delta_f H°(NO_3)$.

$\Delta_f H°(NO_3)$(298 K)	Year	Method	Ref.
17.62 ± 0.33	1992	$D_o(O\text{-}NO_2)$	This work
17.9 ± 0.8	1991	$EA(NO_3)$ + $\Delta_f H°(NO_3^-)$	4
15.39 ± 0.72	1988	K_{eq} + revised $\Delta_f H°(N_2O_5)$	3
17.0 ± 5.0	1985	JANAF Summary	1
17.5 ± 1.0	1985	K_{eq} + $\Delta_f H°(N_2O_5)$	6
17.30 ± 0.7	1984	K_{eq} + $\Delta_f H°(N_2O_5)$	7
17.59 ± 0.2	1978	K_{eq} + $\Delta_f H°(N_2O_5)$	8
17.11 ± 1.0	1958	Shock Pyrolysis	9

Table II: Calculated NO_3 Vibrational Populations Assuming D_{3h} Symmetry

Mode	Vibrational Frequency (cm^{-1})	Degeneracy	$N(v_i=1)/N(v_i=0)$ (300°C)	$N(v_i=1)/N(v_i=0)$ (25°C)
ν_1	1050[42]	1	0.08	0.0066
ν_2	762[43]	1	0.16	0.026
ν_3	1492[19]	2	0.056	0.0016
ν_4	363[6]	2	0.804	0.35

7. LIST OF FIGURES

Fig. 1 NO_3 Absorption Spectrum at 230 and 298 K, obtained from Ref. 17.

Fig. 2 Relevent energy levels for NO_3 photodissociation. Thermodynamic quantitites were obtained from Ref 1. Potential energy barrier for $NO_3(^2A') \rightarrow NO + O_2(^3\Sigma^-_g, ^1\Delta_g)$ obtained in this work.

Fig. 3 Schematic of NO_3 nozzle design.

Fig. 4 Newton diagram in velocity space for photodissociation of NO_3 at photon energy 2 kcal/mole above $D_o(O\text{-}NO_2)$. Arrow indicates measured NO_3 beam velocity and circles denote maximum calculated recoil velocities for NO containing fragments.

Fig. 5 TOF spectra obtained for NO_2^+, NO^+, and O_2^+ products from 590 nm photolysis of NO_3. Angle between the molecular beam and detector was 10°. In NO^+ TOF, the fast peak is due to $NO + O_2$ channel, and the slower peak is NO^+ daughter ion from $NO_2 + O$ channel.

Fig 6 NO^+ TOF from $NO + O_2$ channel obtained at several detector angles from 588 nm photolysis of NO_3.

Fig 7 NO^+ and O^+ TOF from $NO_2 + O$ channel from 588 nm photolysis of NO_3. Small contribution in O^+ TOF signal at 6° is from fragmentation of NO_2 to O^+ in ionizer.

Fig 8 Product translational energy distribution for the $NO + O_2$ channel from NO_3 photodissociation at 588 nm. The calculated maximum relative translational energies for production of $NO(v=0) + O_2(^3\Sigma, ^1\Delta)$ (v') are indicated.

Fig 9 Product translational energy distributions for the $NO_2 + O$ channel from NO_3 photodissociation at 588 nm.

Fig 10 NO^+ TOF spectra at several excitation wavelengths. The angle between the detector and molecular beam was 10°.

Fig 11 ■ - Integrated Intensity of the $NO + O_2$ TOF signal at various excitation wavelengths. The NO_3 absorption spectrum (Ref 17) at two temperatures is also shown.

Fig 12 NO^+ and O^+ TOF spectra from $NO_3 \rightarrow NO_2 + O$ at 570 nm. The angle between the molecular beam and detector is indicated.

Fig 13 P(E) for $NO_2 + O$ channel at 570 nm. Arrow denotes maximum calculated translational energy release from photodissociation of cold NO_3.

Fig 14 NO^+ and O^+ TOF spectra from $NO_3 \rightarrow NO_2 + O$ at 548 nm. The angle between the molecular beam and detector is indicated.

Fig 15 P(E) for $NO_2 + O$ channel at 548 nm. Arrow denotes maximum calculated translational energy release from photodissociation of cold NO_3.

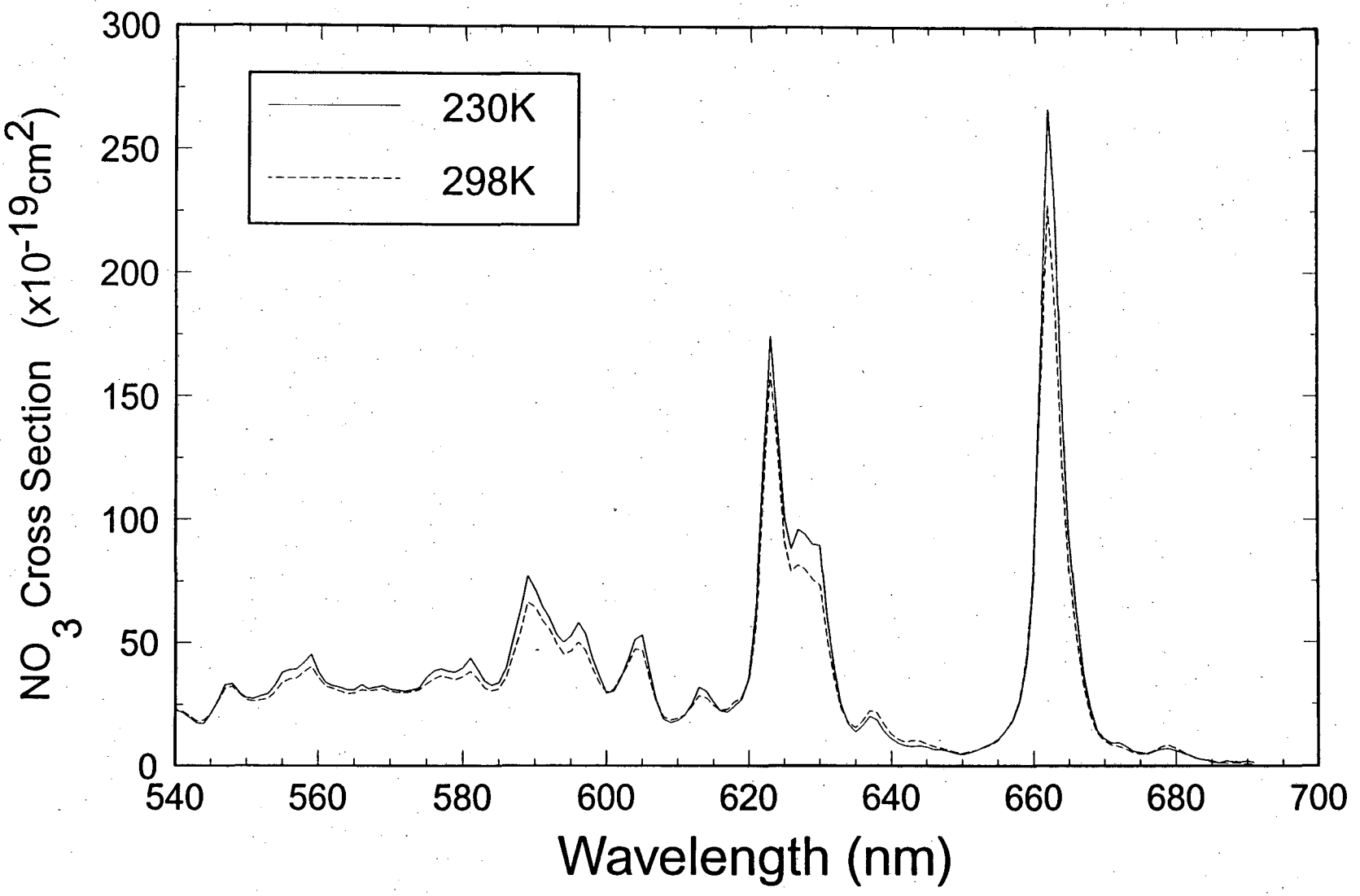
230K
298K
NO_3 Cross Section ($x10^{-19}cm^2$)
Wavelength (nm)
0
50
100
150
200
250
300
540
560
580
600
620
640
660
680
700

Fig. 1

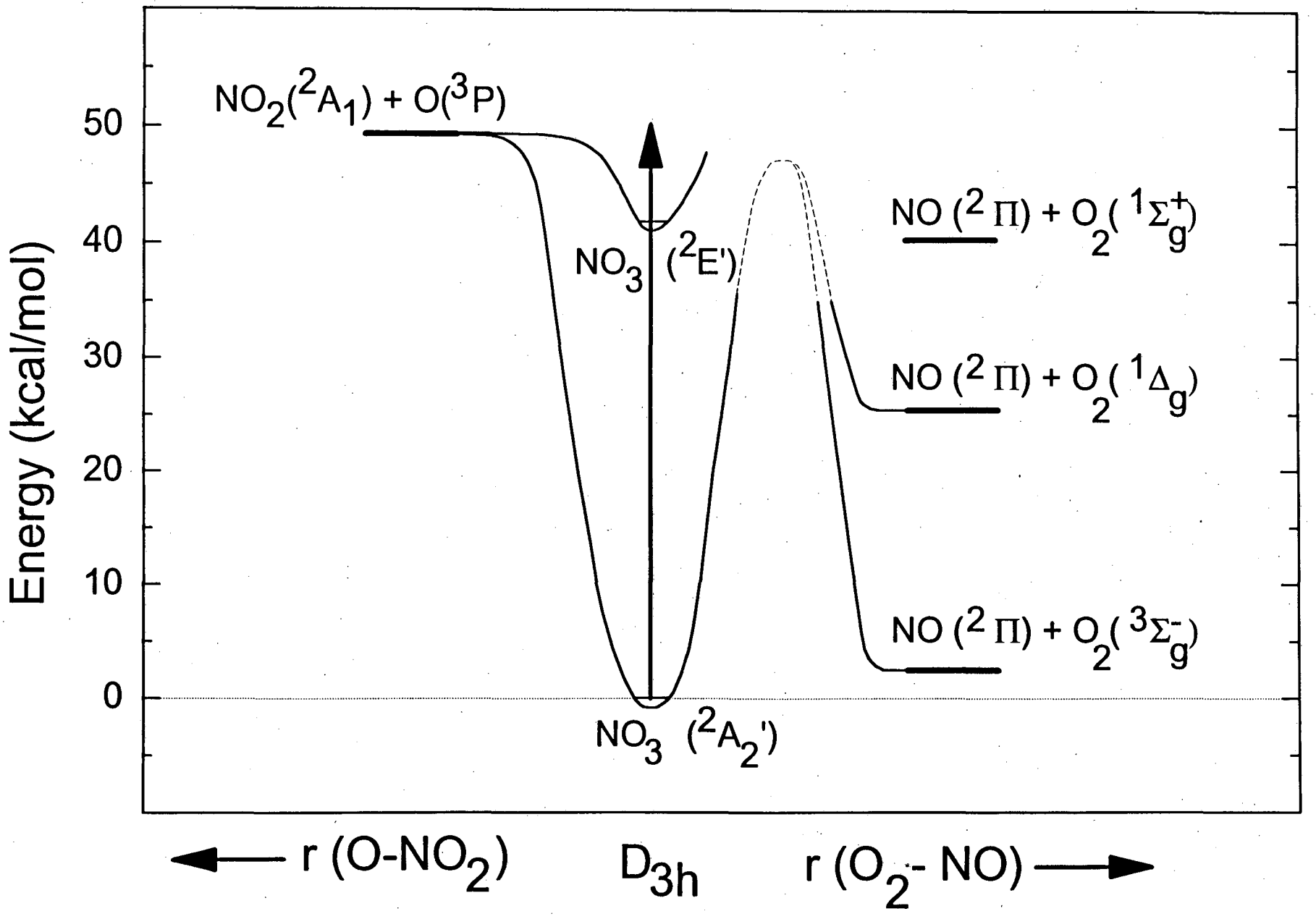
Energy (kcal/mol)
50
40
30
20
10
0
$NO_2(^2A_1) + O(^3P)$
NO_3 $(^2E')$
NO_3 $(^2A_2')$
NO ($^2\Pi$) + O_2($^1\Sigma_g^+$)
NO ($^2\Pi$) + O_2($^1\Delta_g$)
NO ($^2\Pi$) + O_2($^3\Sigma_g^-$)
r (O-NO_2)
D_{3h}
r (O_2- NO)

Fig. 2

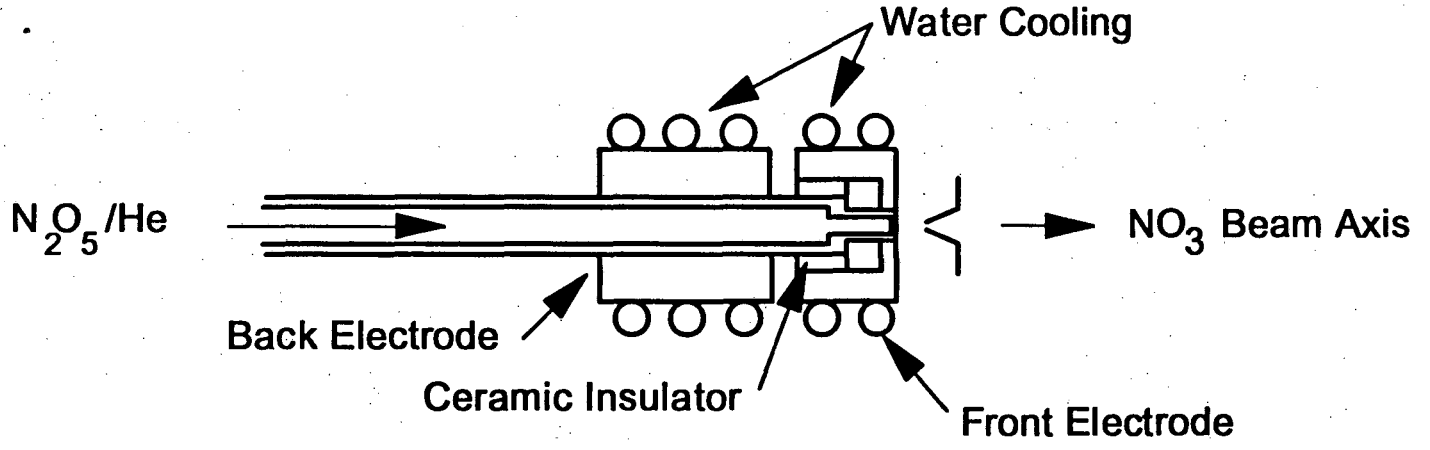
Water Cooling
N_2O_5/He
NO_3 Beam Axis
Back Electrode
Ceramic Insulator
Front Electrode

Fig. 3

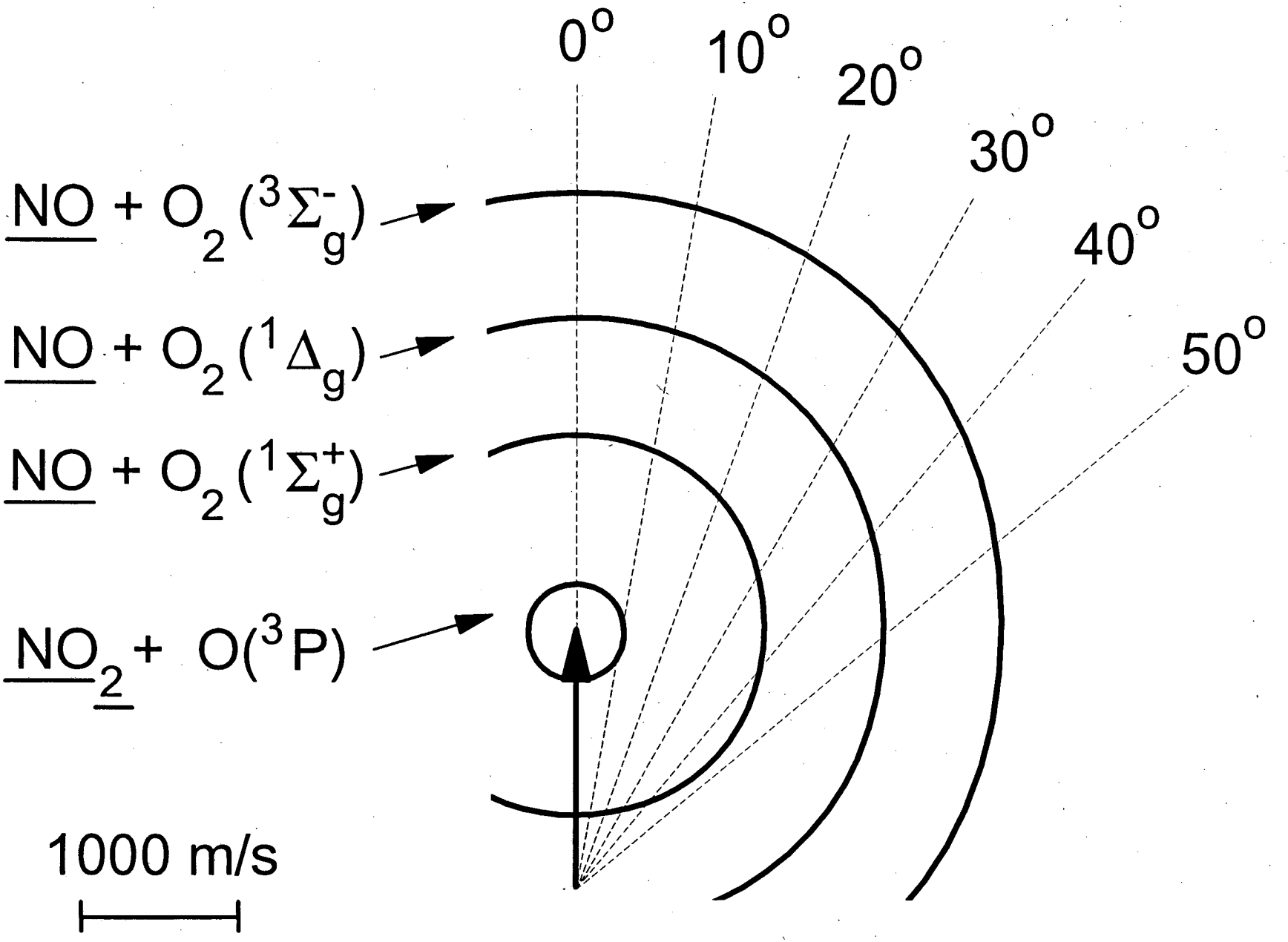

Fig. 4

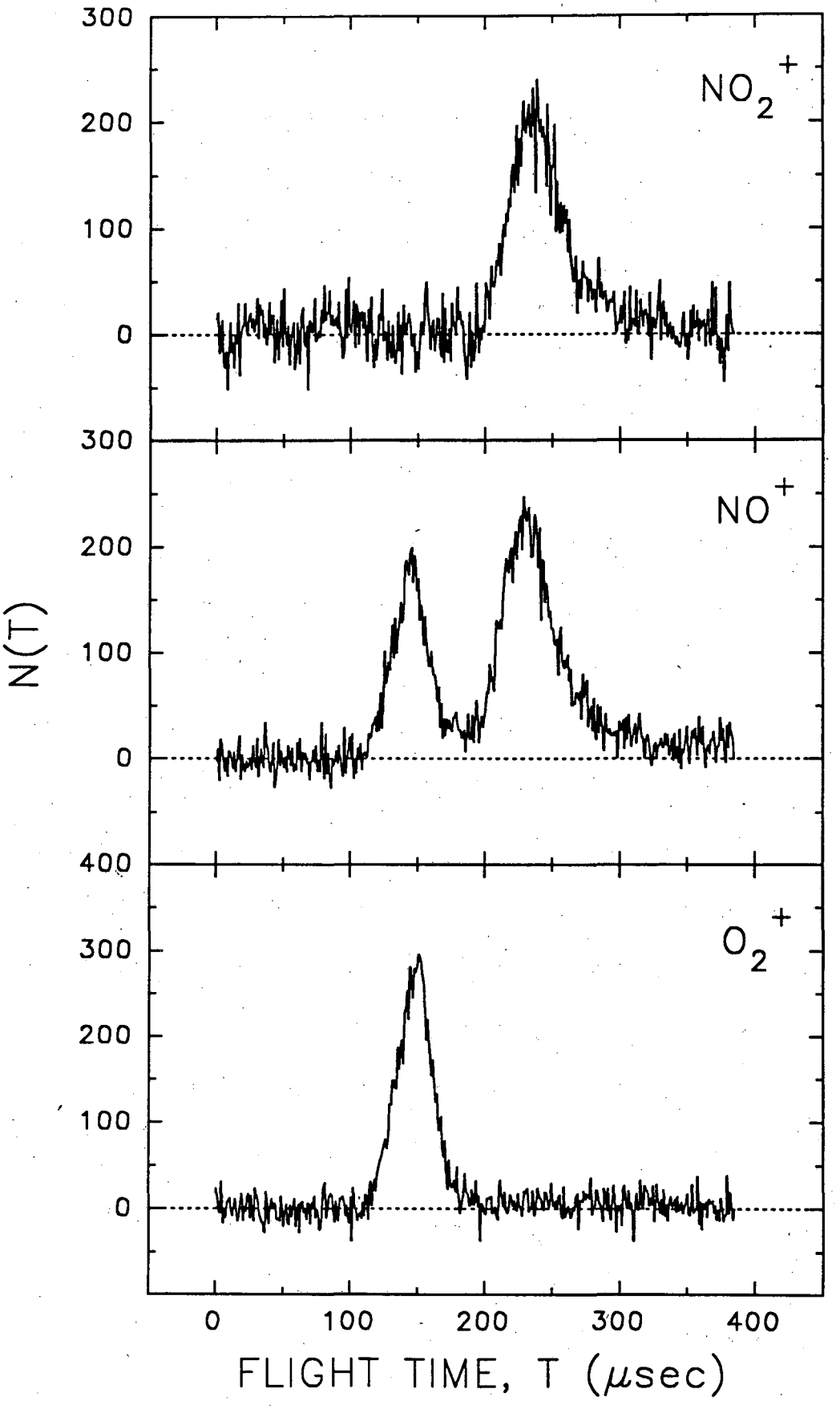
300
200
100
0
NO_2^+
300
200
100
0
NO^+
400
300
200
100
0
O_2^+
N(T)
0
100
200
300
400
FLIGHT TIME, T (μsec)

Fig. 5

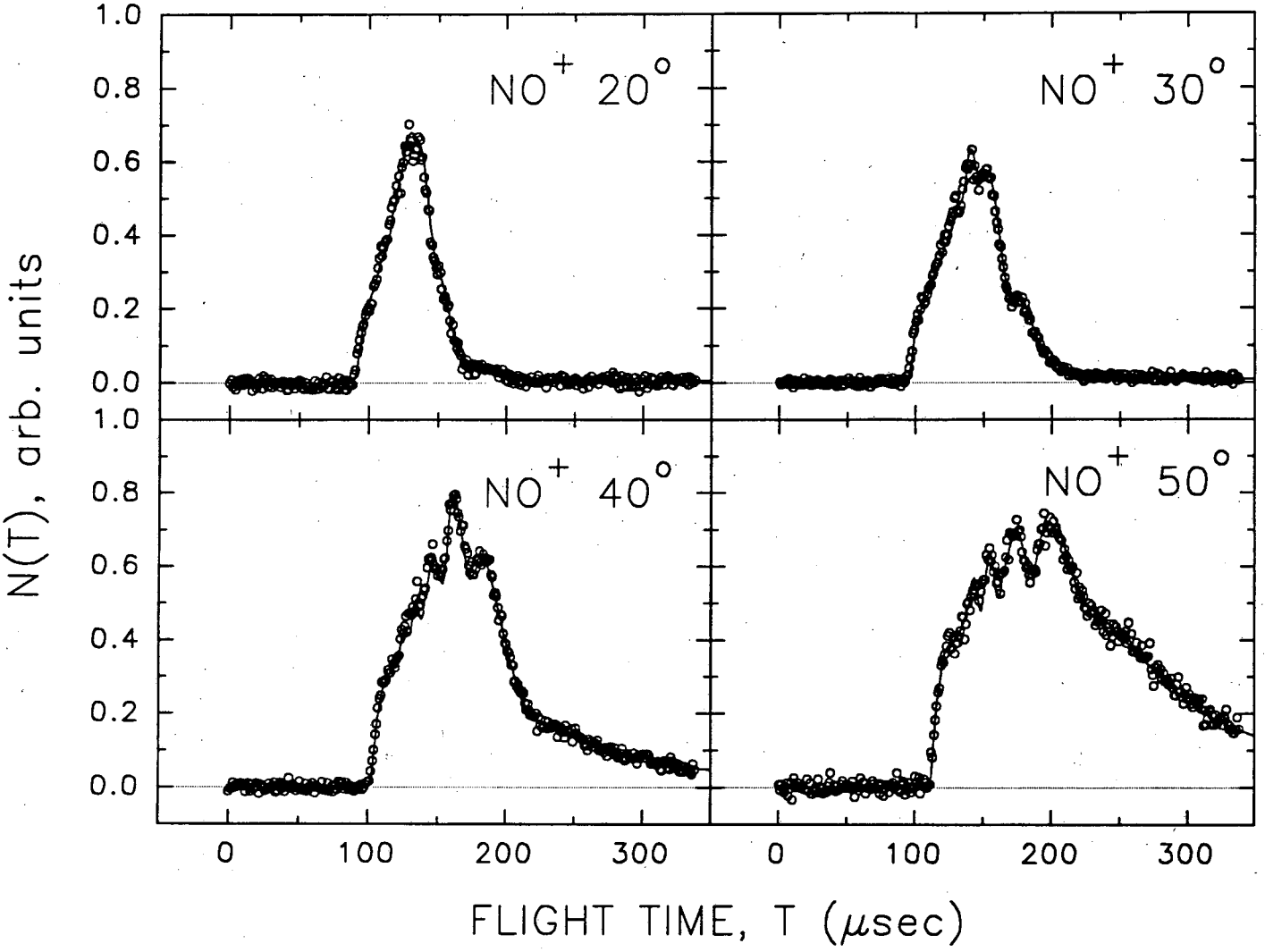
NO+ 20°
NO+ 30°
NO+ 40°
NO+ 50°
N(T), arb. units
FLIGHT TIME, T (μsec)
0.0
0.2
0.4
0.6
0.8
1.0
0
100
200
300

Fig. 6

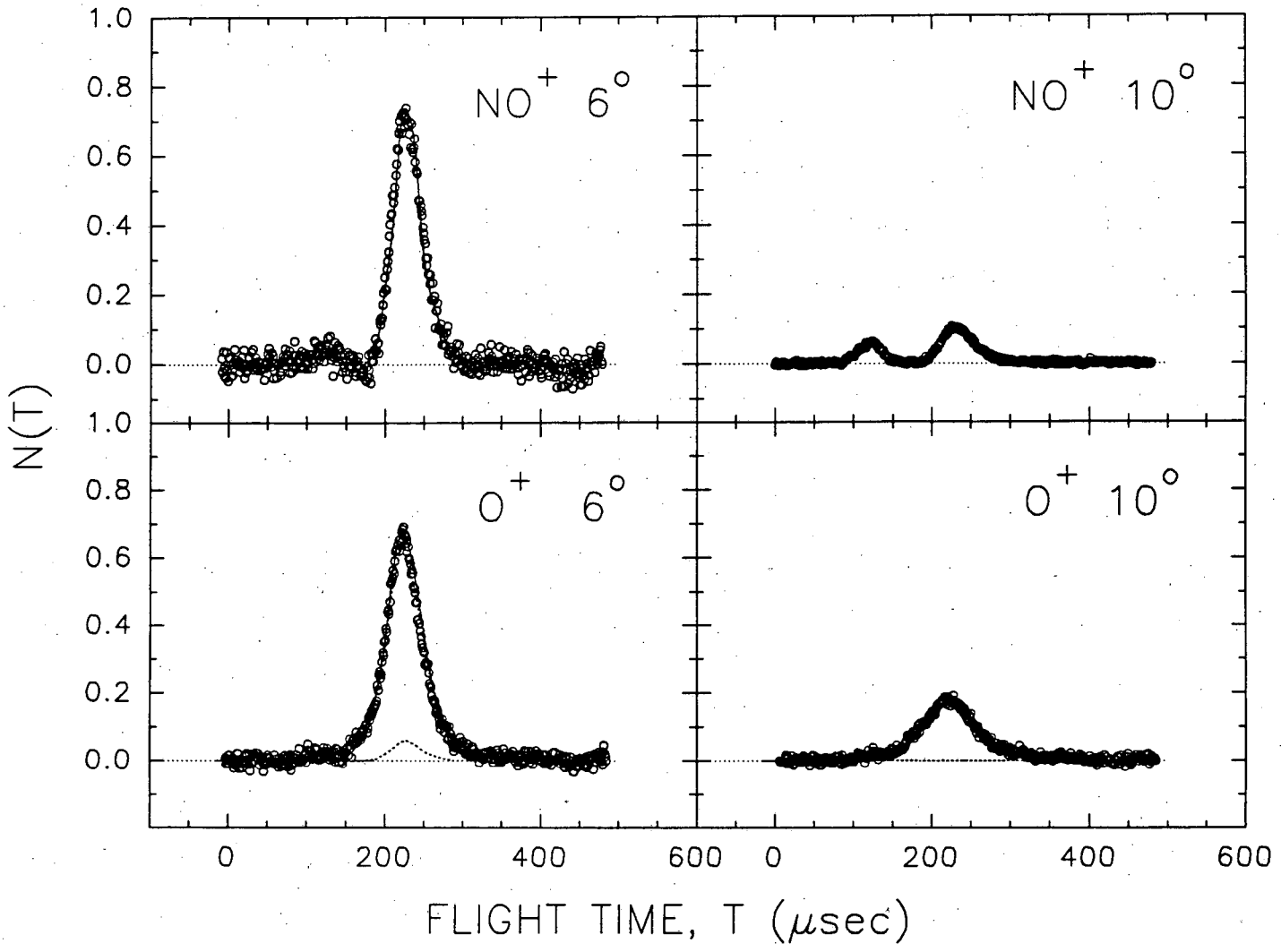
1.0
0.8
0.6
0.4
0.2
0.0
N(T)
NO+ 6°
NO+ 10°
O+ 6°
O+ 10°
0
200
400
600
FLIGHT TIME, T (μsec)

Fig. 7

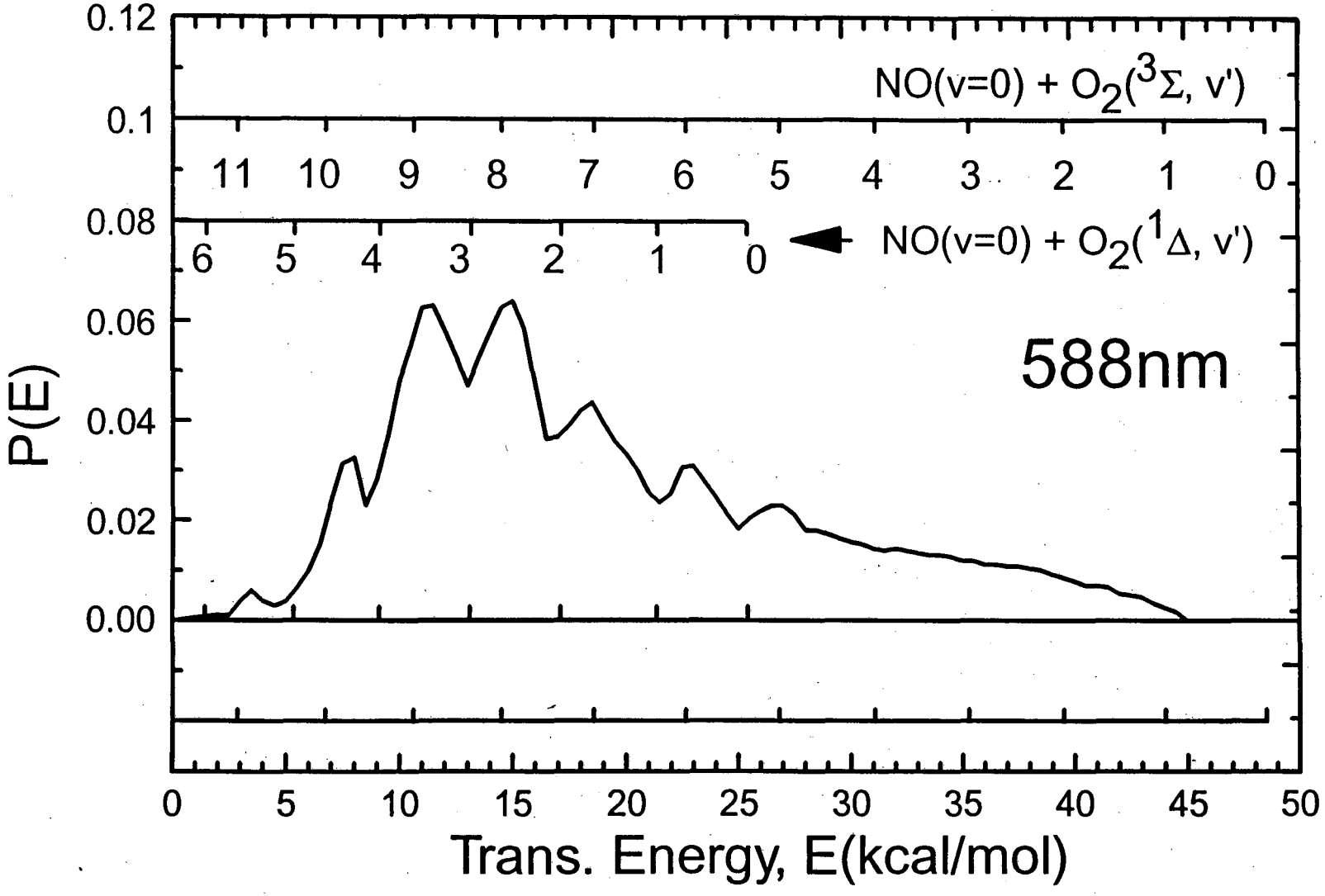
0.12
0.1
0.08
0.06
0.04
0.02
0.00
P(E)
NO(v=0) + O2(3Σ, v')
11 10 9 8 7 6 5 4 3 2 1 0
6 5 4 3 2 1 0
NO(v=0) + O2(1Δ, v')
588nm
0 5 10 15 20 25 30 35 40 45 50
Trans. Energy, E(kcal/mol)

Fig. 8

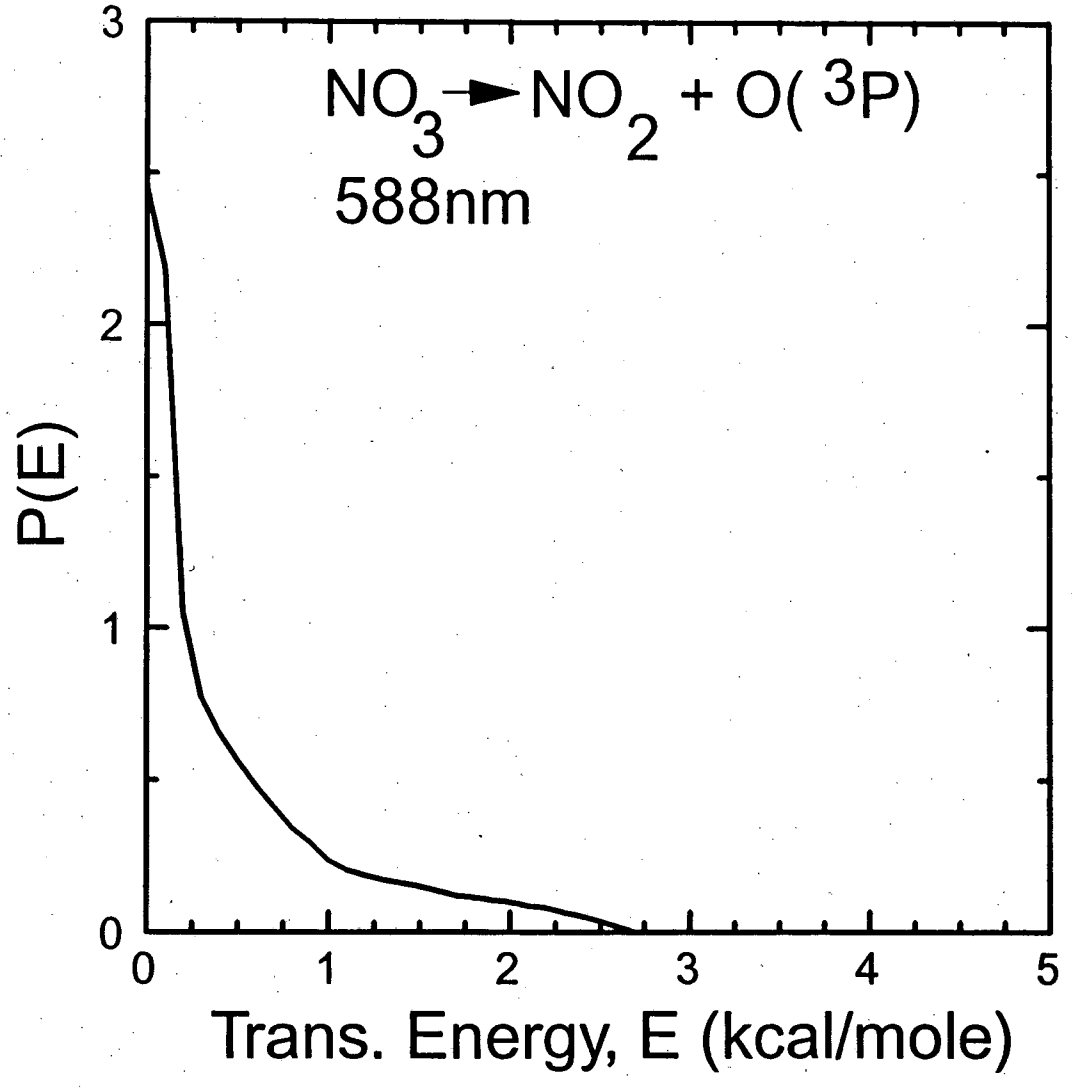

Fig 9

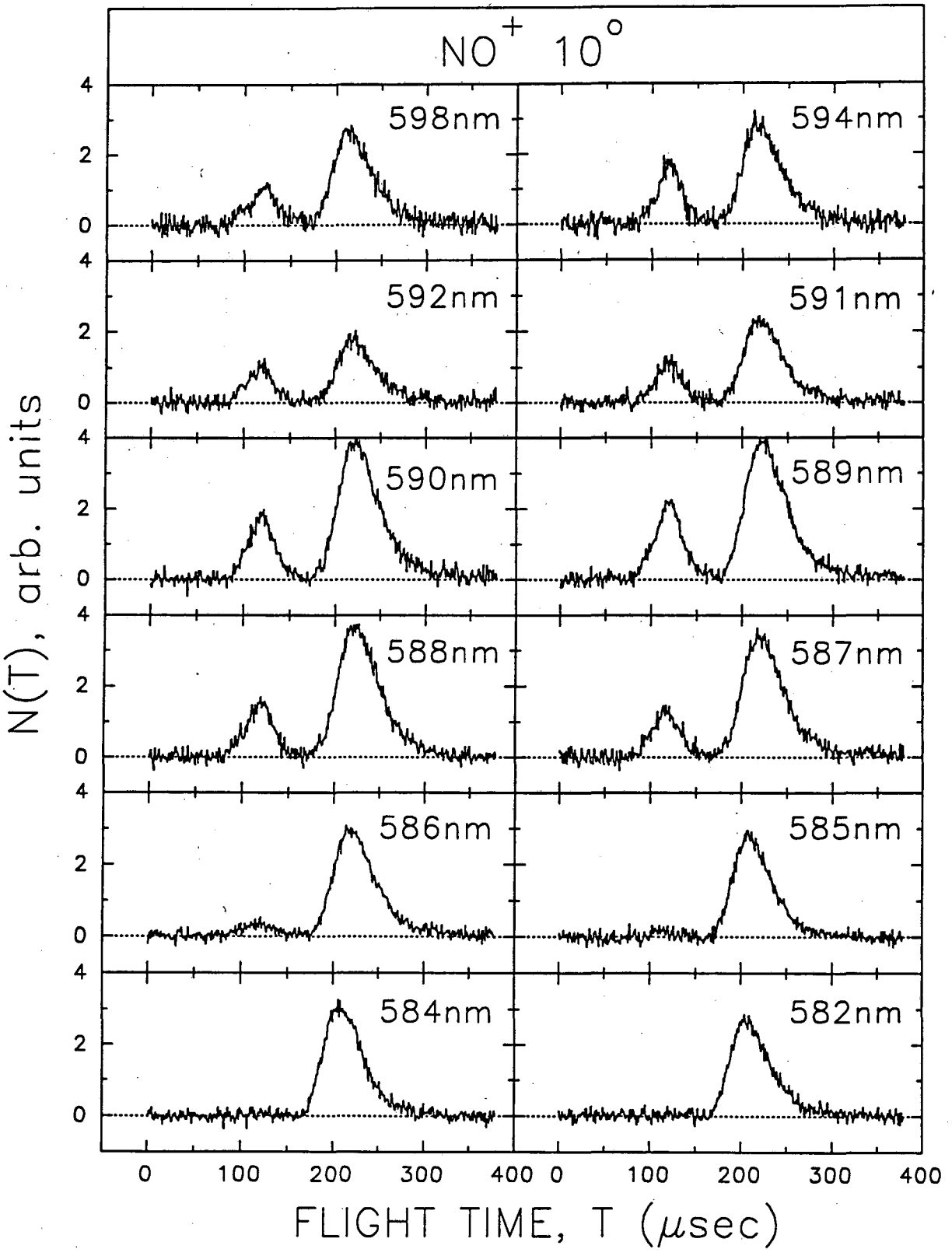
NO+ 10°
598nm
594nm
592nm
591nm
590nm
589nm
588nm
587nm
586nm
585nm
584nm
582nm
N(T), arb. units
FLIGHT TIME, T (μsec)
0
100
200
300
400
2
4

Fig. 10

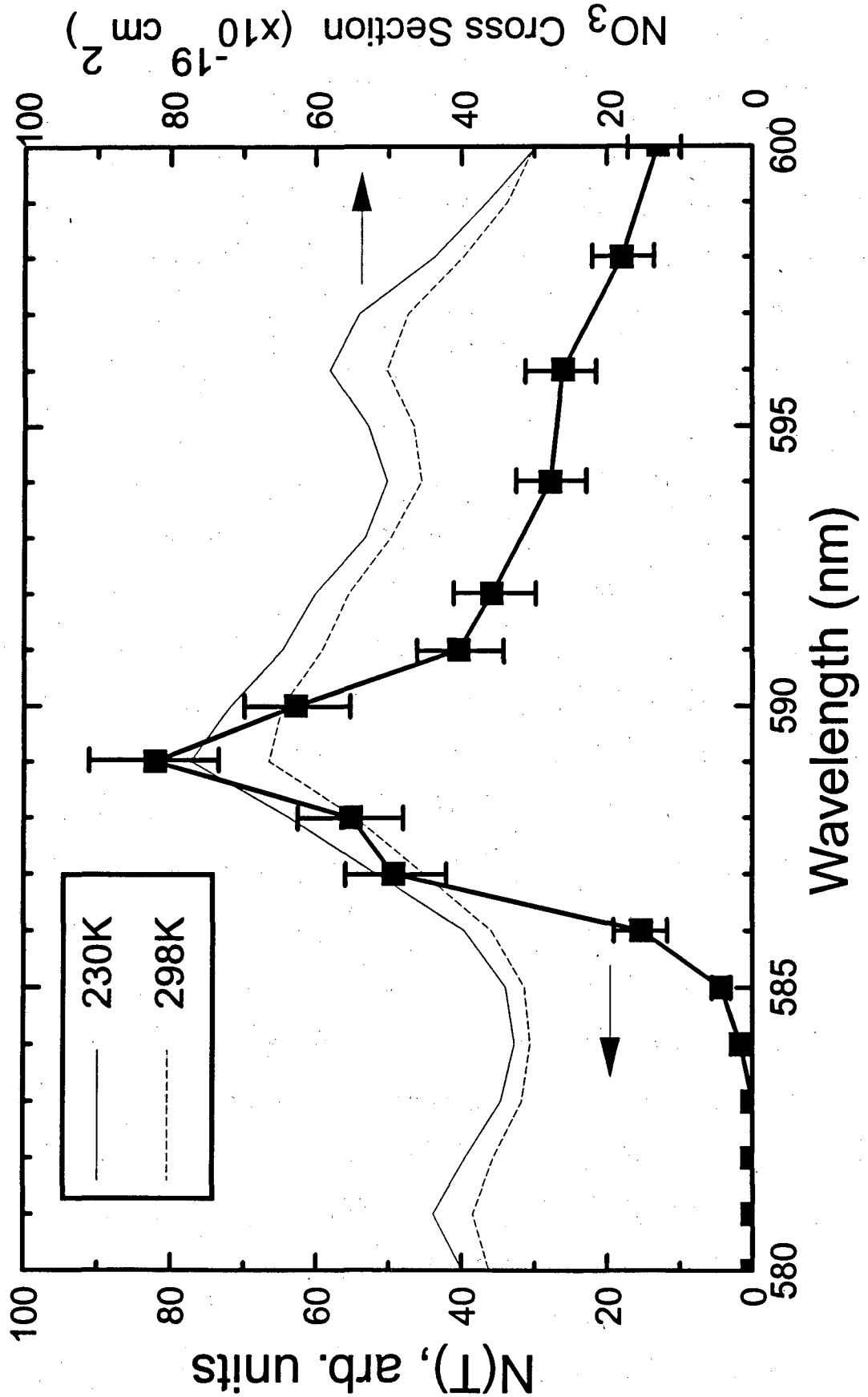
N(T), arb. units
Wavelength (nm)
NO3 Cross Section (x10-19 cm2)
230K
298K
0
20
40
60
80
100
580
585
590
595
600

Fig. 11

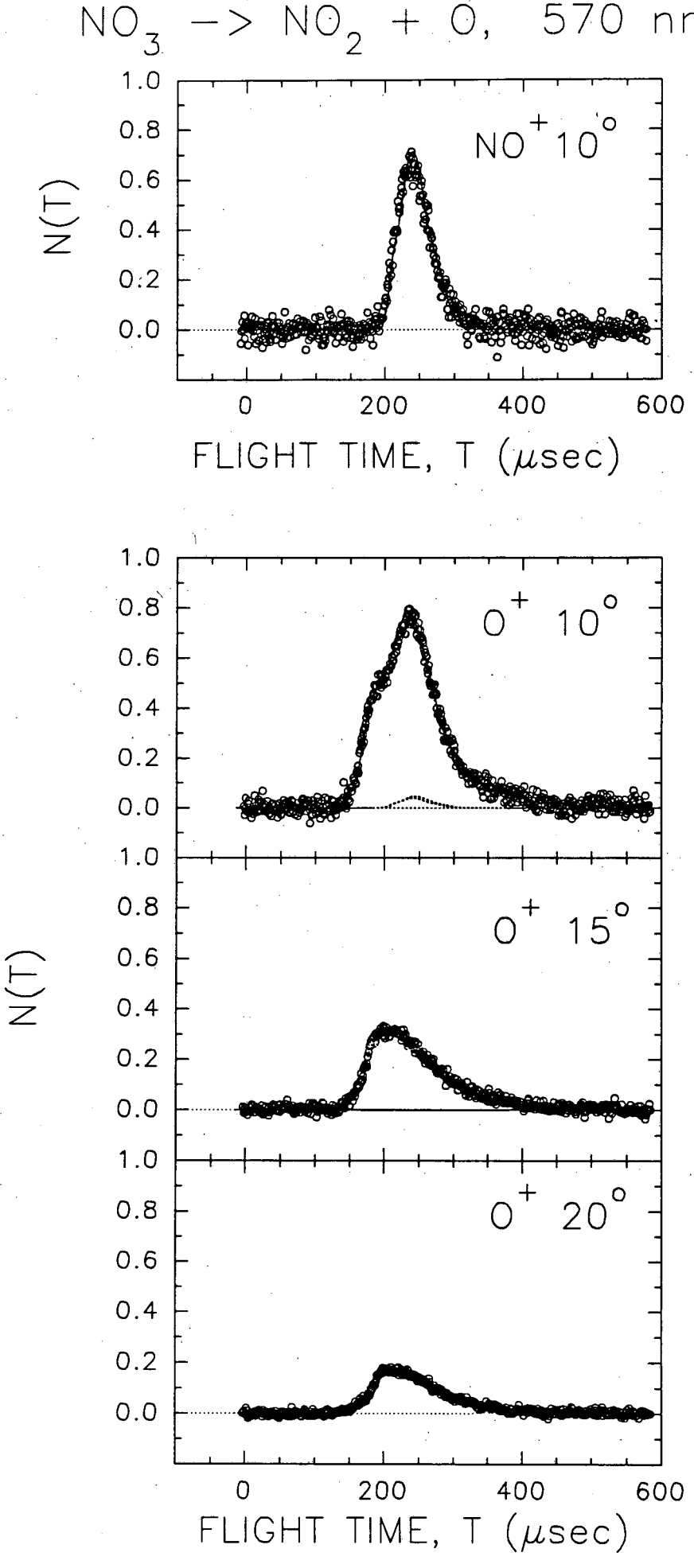
NO3 -> NO2 + O, 570 nm
NO+ 10°
O+ 10°
O+ 15°
O+ 20°
N(T)
FLIGHT TIME, T (μsec)
0
200
400
600
0.0
0.2
0.4
0.6
0.8
1.0

Fig. 12

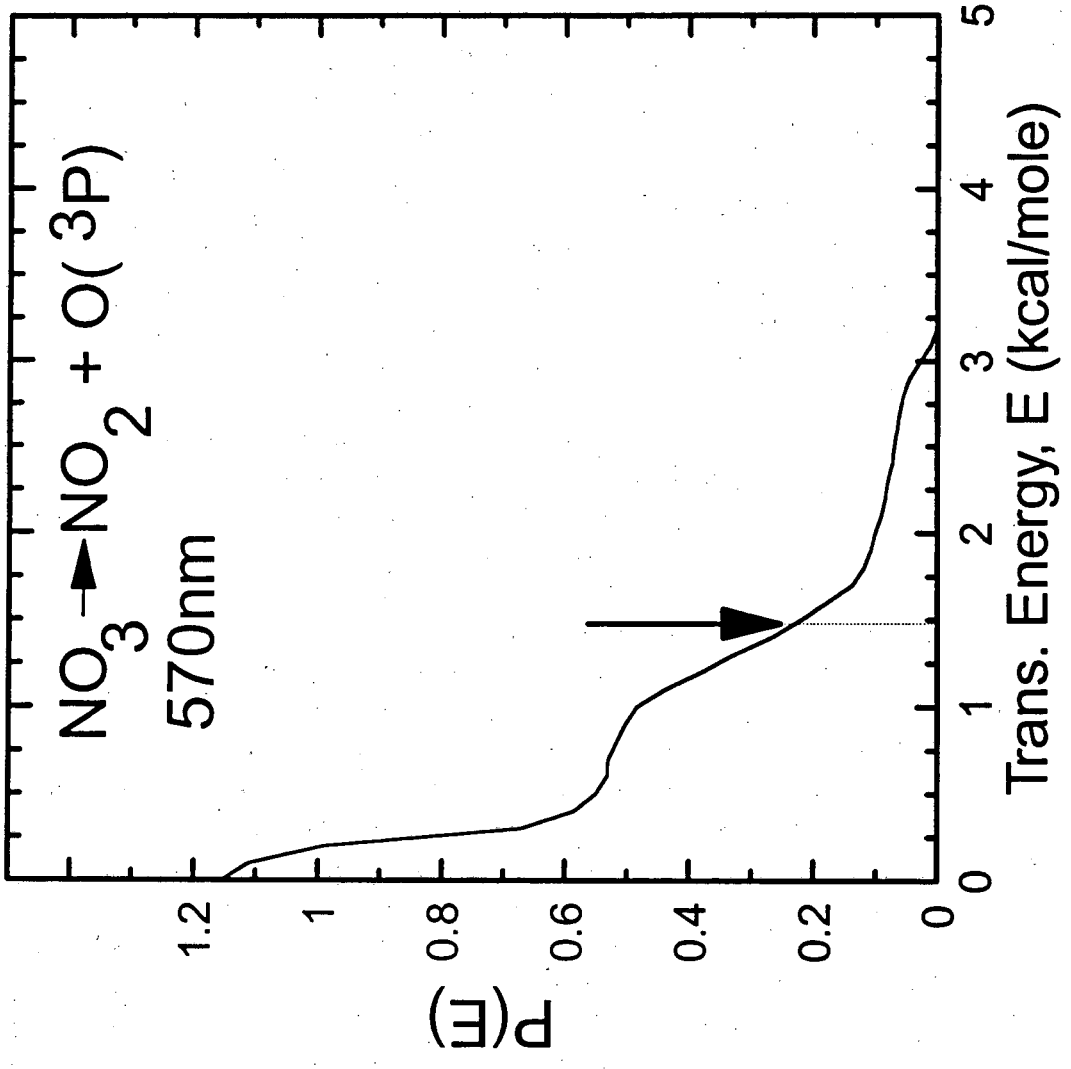
NO3→NO2 + O(3P)
570nm
P(E)
Trans. Energy, E (kcal/mole)
0
0.2
0.4
0.6
0.8
1
1.2
0
1
2
3
4
5

Fig 13

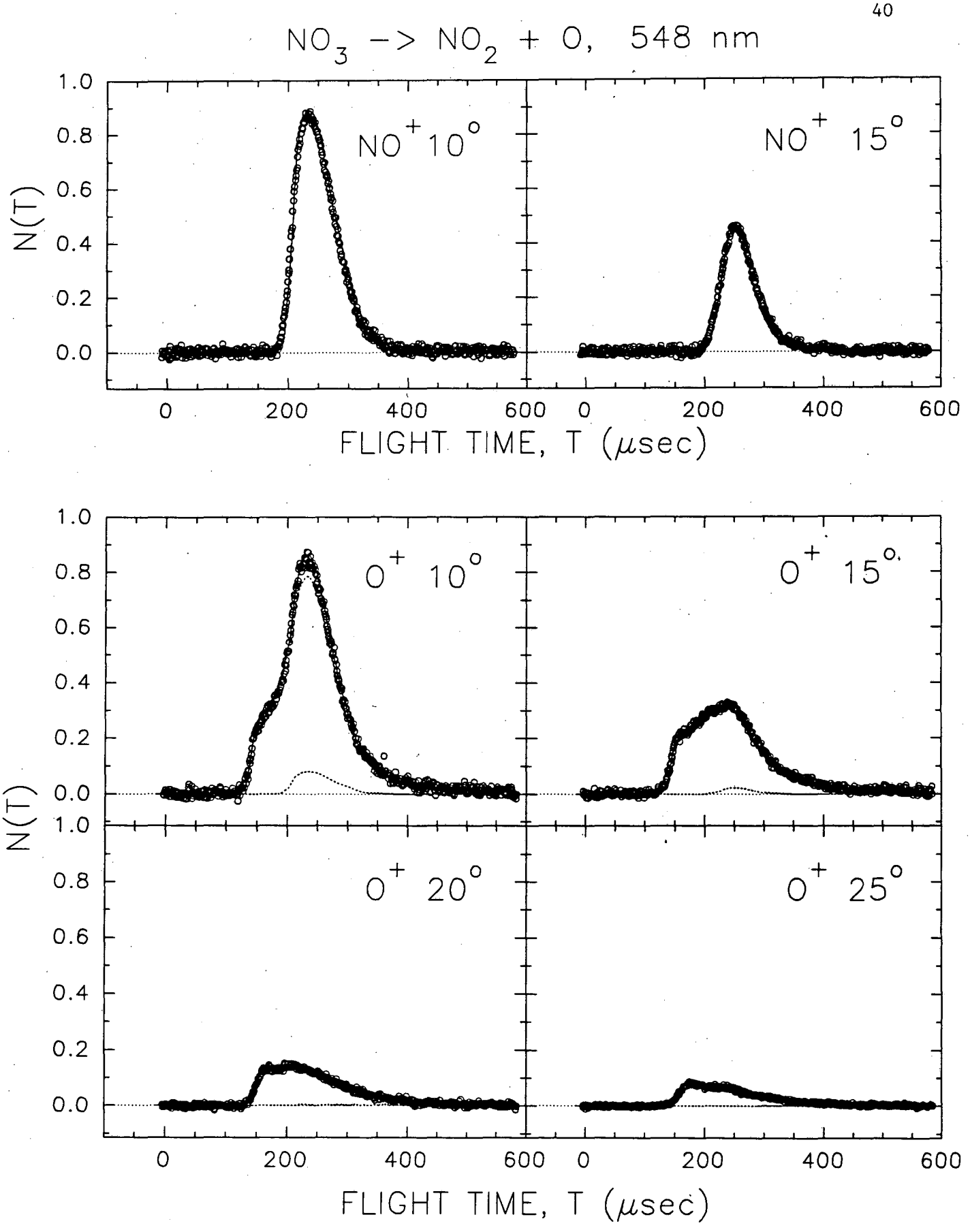
NO3 -> NO2 + O, 548 nm
NO+ 10°
NO+ 15°
O+ 10°
O+ 15°
O+ 20°
O+ 25°
N(T)
1.0
0.8
0.6
0.4
0.2
0.0
0
200
400
600
FLIGHT TIME, T (μsec)

Fig. 14

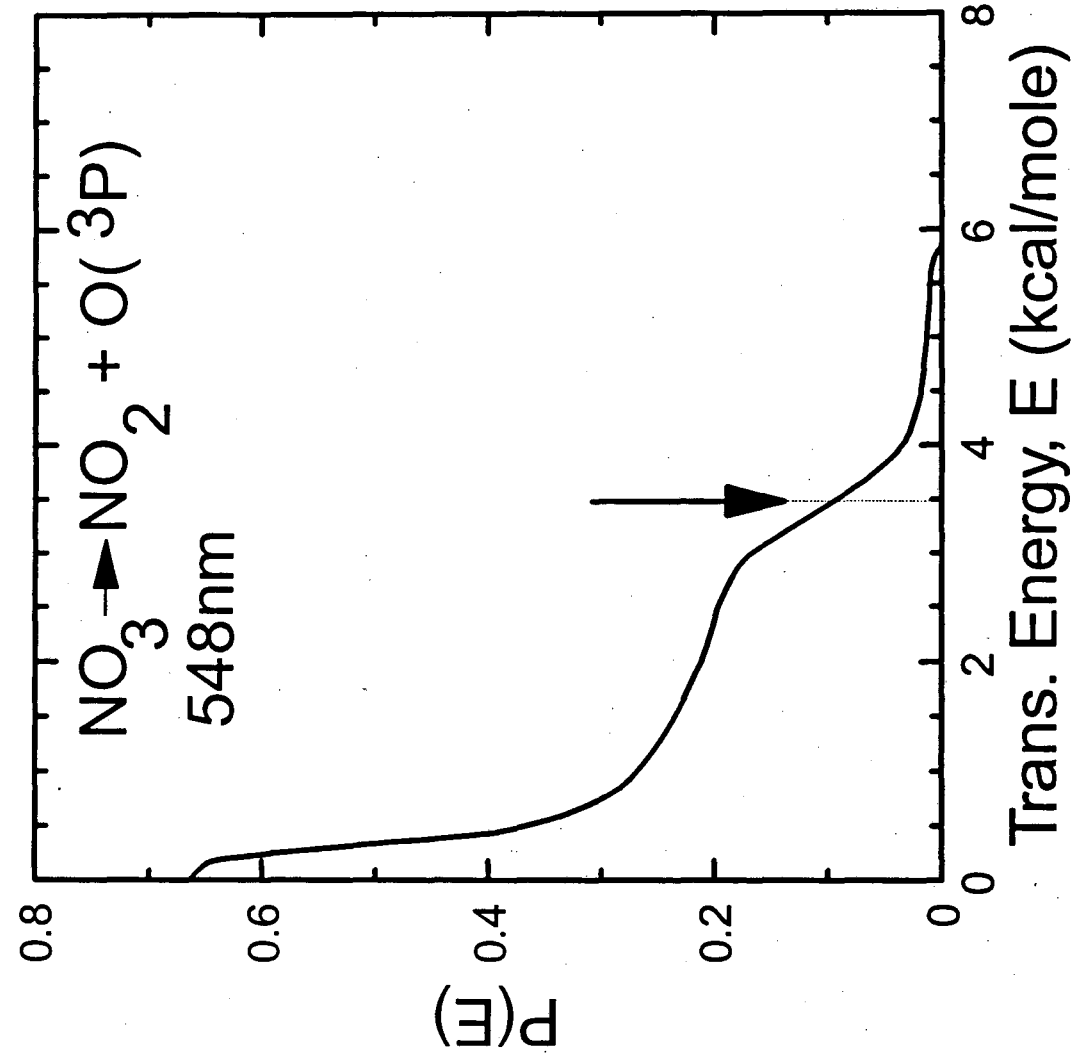
$NO_3 \rightarrow NO_2 + O(^3P)$
548nm
P(E)
Trans. Energy, E (kcal/mole)
0
0.2
0.4
0.6
0.8
2
4
6
8

Fig 15

LAWRENCE BERKELEY LABORATORY
UNIVERSITY OF CALIFORNIA
TECHNICAL INFORMATION DEPARTMENT
BERKELEY, CALIFORNIA 94720